

EFFICIENT AND ACCURATE EXPONENTIAL SAV ALGORITHMS WITH RELAXATION FOR DISSIPATIVE SYSTEM *

YANRONG ZHANG[†] AND XIAOLI LI[‡]

Abstract. In this paper, we construct two kinds of exponential SAV approach with relaxation (R-ESAV) for dissipative system. The constructed schemes are linear and unconditionally energy stable. They can guarantee the positive property of SAV without any assumption compared with R-SAV and R-GSAV approaches, preserve all the advantages of the ESAV approach and satisfies dissipation law with respect to a modified energy which is directly related to the original free energy. Moreover the second version of R-ESAV approach is easy to construct high-order BDF k schemes. Especially for Navier-Stokes equations, we construct two kinds of novel schemes based on the R-ESAV method. Finally, ample numerical examples are presented to exhibit that the proposed approaches are accurate and effective.

Key words. dissipative system; energy stability; exponential scalar auxiliary variable (ESAV); relaxation

AMS subject classifications. 35Q40; 65M12; 35Q55; 65M70

1. Introduction. Many significant scientific and engineering problems, such as complex fluids, new composite materials, the non-convex function optimization, etc., can be modeled by the dissipative system. From the numerical perspective, it's critical to maintain the discrete energy dissipation law so as to obviate non-physical numerical solutions. Over the past few decades, a large effort has been devoted to construct efficient energy stable time discretized schemes for the dissipative system. Existing and popular approaches can be classified into several categories: stabilized linearly implicit approach [35, 26], exponential time differencing (ETD) approach [28, 7, 8], convex splitting approach [9, 10, 22, 1], invariant energy quadratization (IEQ) approach [30, 32, 33, 27], scalar auxiliary variable (SAV) approach [24, 23, 25] and so on.

Among these approaches, SAV method has become a very efficient and popular tool to construct energy stable schemes and has been successfully applied to gradient flow [24, 25, 6, 18, 27] and general dissipative systems [19, 16, 17]. SAV method possesses a lot of attractive superiorities, but there are still some deficiencies that need to be improved. For example, (i) it requires to solve two linear systems at each time step; (ii) it requires that nonlinear part of free energy has a lower bound; (iii) it satisfies unconditional energy stability according to modified energy rather than original energy. Recently there have been some corresponding improvements for these shortcomings. A generalized SAV approach which only requires solving one linear equation with constant coefficients has been proposed by Huang et al. [13, 12]. Cheng et al. [2, 5] proposed a novel Lagrange multiplier approach which dissipates original energy and do not require the nonlinear part of the free energy to be bounded from below. The constructed scheme requires solving a nonlinear algebraic equation which brings some additional computation costs and theoretical analysis difficulties, and may not exist a suitable solution when the time step is insufficiently small. Besides, some SAV approaches in more general form have been developed to extend its applicability in [20, 21, 3]. The constructed schemes, especially for the exponential SAV methods, don't need to require that the nonlinear part of the free energy has a lower bound and can guarantee the positive property of SAV without any assumption. Very recently, the relaxation technique has been adopted to the SAV approach to improve the accuracy of numerical solutions in [14, 34]. The key idea in this approach is to make the modified energy link to the original energy closely by updating the auxiliary variable.

*This work is supported by the National Natural Science Foundation of China grants 12271302, 12131014 and 11971407.

[†] Department of Applied Mathematics, The Hong Kong Polytechnic University, Hung Hom, Hong Kong. Email: yanrongzhang_math@163.com.

[‡]Corresponding Author. School of Mathematics, Shandong University, Jinan, 250100, China. Email: xiaoli-math@sdu.edu.cn.

Our aim in this paper is to propose two kinds of relaxed exponential SAV (R-ESAV) approaches for dissipative system. The constructed schemes directly link the SAV to the free energy by introducing relaxation technique, and have outstanding advantages in the following aspects:

- R-ESAV schemes are unconditionally energy stable with regard to a modified energy which is closer and directly linked to the original free energy, and can improve the accuracy of the solution noticeably compared with the original ESAV approach;
- Only one linear system with constant coefficients needs to be solved;
- The constructed schemes do not need the bounded below limitation of the nonlinear part of free energy;
- The positive property of SAV without any assumption can be guaranteed.

In addition, our numerical results show that, R-ESAV schemes can improve the accuracy of SAV ξ^{n+1} , and for the plenty numerical simulations that we tested, the modified energy of our R-ESAV schemes all most always equals to the original free energy. Moreover, two kinds of BDF k ($1 \leq k \leq 4$) numerical schemes based on two different decoupled approaches are constructed for Navier-Stokes equations. To the author's knowledge, it is the first time to apply relaxation technique to the general dissipative systems.

The remainder of this paper is organized as follows. In Section 2, we present the first version of relaxed exponential SAV approach for gradient flow. Then we extend the R-ESAV-1 approach to gradient systems with multiple components or multiple nonlinear potentials. In Section 3, we give the second version of relaxed exponential SAV approach for general dissipative system and construct two BDF k schemes for Navier-Stokes equation. In Section 4, we present several numerical experiments by using the new approaches, and provide ample numerical simulations to validates its generality and efficiency. In Section 5, we provide some concluding remarks.

2. The first version of relaxed exponential SAV approach. In this section, we consider the improvement of ESAV approach [20] by introducing a relaxation factor to modified the SAV, which is abbreviated as R-ESAV-1 approach for convenience.

2.1. The R-ESAV-1 approach for gradient flow. Without losing generality, we consider a free energy given by

$$(2.1) \quad E(\phi) = \frac{1}{2}(\mathcal{L}\phi, \phi) + \int_{\Omega} F(\phi) d\mathbf{x},$$

where \mathcal{L} is a self-adjoint linear elliptic operator, $F(\phi)$ is a nonlinear energy density function. Then, the gradient flow derived from the above free energy by energy-variational principle can be written as follows

$$(2.2) \quad \begin{cases} \frac{\partial \phi}{\partial t} = -\mathcal{G}\mu, \\ \mu = \frac{\delta E(\phi)}{\delta \phi} = \mathcal{L}\phi + F'(\phi), \end{cases}$$

where \mathcal{G} is a positive definite operator which signifies the dissipative mechanism of the system, e.g. $\mathcal{G} = I$ for the L^2 gradient flow and $\mathcal{G} = -\Delta$ for the H^{-1} gradient flow.

We introduce an exponential SAV

$$(2.3) \quad r(t) = \exp(E_1(\phi)) = \exp\left(\int_{\Omega} F(\phi) d\mathbf{x}\right),$$

and by taking the derivative of (2.3) with respect to t , we have

$$(2.4) \quad \frac{dr}{dt} = r \int_{\Omega} F'(\phi) \phi_t d\mathbf{x} = \frac{r^2}{\exp(E_1(\phi))} \int_{\Omega} F'(\phi) \phi_t d\mathbf{x}.$$

Denote $U(r, \phi) = \frac{r}{\exp(E_1(\phi))} F'(\phi)$, and notice that equation (2.4) can be rewritten equivalently into

$$(2.5) \quad \frac{d \ln(r)}{dt} = (U(r, \phi), \phi_t),$$

then we rewrite the system (2.2) as follows

$$(2.6) \quad \begin{cases} \frac{\partial \phi}{\partial t} = -\mathcal{G}\mu, \\ \mu = \mathcal{L}\phi + U(r, \phi), \\ \frac{d \ln(r)}{dt} = (U(r, \phi), \phi_t). \end{cases}$$

By taking the inner product of the first two equations in (2.6) with μ and $\frac{\partial \phi}{\partial t}$, respectively, we have

$$(2.7) \quad \frac{d}{dt} \left[\frac{1}{2} (\mathcal{L}\phi, \phi) + \ln(r) \right] = -(\mathcal{G}\mu, \mu) \leq 0.$$

Inspired by the idea of relaxation factor in [14, 34], we can construct R-ESAV-1/BDF k ($1 \leq k \leq 6$) schemes:

Given $r^{n-k}, \dots, r^n, \phi^{n-k}, \dots, \phi^n$, we determine r^{n+1}, ϕ^{n+1} via two steps as follows:

Step 1: Compute an intermediate solution $(\tilde{r}^{n+1}, \phi^{n+1})$ by using the ESAV approach:

$$(2.8) \quad \frac{\alpha_k \phi^{n+1} - A_k(\phi^n)}{\delta t} = -\mathcal{G}\mu^{n+1},$$

$$(2.9) \quad \mu^{n+1} = \mathcal{L}\phi^{n+1} + U(B_k(r^n), B_k(\phi^n)),$$

$$(2.10) \quad \frac{\alpha_k \ln(\tilde{r}^{n+1}) - A_k(\ln(r^n))}{\delta t} = \left(U(B_k(r^n), B_k(\phi^n)), \frac{\alpha_k \phi^{n+1} - A_k(\phi^n)}{\delta t} \right),$$

where α_k, A_k and B_k are related parameter and operators of BDF k schemes, which can be obtained by Taylor expansion. For the convenience of readers, we provide the form of $k = 1, 2, 3, 4$ as follows:

First-order:

$$(2.11) \quad \alpha_1 = 1, \quad A_1(\phi^n) = \phi^n, \quad B_1(\phi^n) = \phi^n;$$

Second-order:

$$(2.12) \quad \alpha_2 = \frac{3}{2}, \quad A_2(\phi^n) = 2\phi^n - \frac{1}{2}\phi^{n-1}, \quad B_2(\phi^n) = 2\phi^n - \phi^{n-1};$$

Third-order:

$$(2.13) \quad \alpha_3 = \frac{11}{6}, \quad A_3(\phi^n) = 3\phi^n - \frac{3}{2}\phi^{n-1} + \frac{1}{3}\phi^{n-2}, \quad B_3(\phi^n) = 3\phi^n - 3\phi^{n-1} + \phi^{n-2};$$

Fourth-order:

$$(2.14) \quad \begin{aligned} \alpha_4 &= \frac{25}{12}, \quad A_4(\phi^n) = 4\phi^n - 3\phi^{n-1} + \frac{4}{3}\phi^{n-2} - \frac{1}{4}\phi^{n-3}, \\ B_4(\phi^n) &= 4\phi^n - 6\phi^{n-1} + 4\phi^{n-2} - \phi^{n-3}. \end{aligned}$$

Step 2: Update r^{n+1} via relaxation factor as follows:

$$(2.15) \quad r^{n+1} = \theta_0^{n+1} \tilde{r}^{n+1} + (1 - \theta_0^{n+1}) \exp(E_1(\phi^{n+1})), \quad \theta_0^{n+1} \in \mathcal{W},$$

where, \mathcal{W} is a set defined as follows:
First-order:

$$(2.16) \quad \mathcal{W} = \{ \theta \in [0, 1] \text{ s.t. } \ln(r^{n+1}) - \ln(\tilde{r}^{n+1}) \leq \delta t \gamma (\mathcal{G}\mu^{n+1}, \mu^{n+1}) \};$$

Second-order:

$$(2.17) \quad \mathcal{W} = \left\{ \theta \in [0, 1] \text{ s.t. } \frac{3}{2} \ln(r^{n+1}) - \frac{3}{2} \ln(\tilde{r}^{n+1}) \leq \delta t \gamma (\mathcal{G}\mu^{n+1}, \mu^{n+1}) \right\};$$

with $\gamma \in [0, 1]$ is a adjustable parameter.

We explain below how to choose θ_0^{n+1} . For BDF1 scheme, plugging (2.15) into (2.16), we derive that if we choose θ_0^{n+1} such that

$$(2.18) \quad (\tilde{r}^{n+1} - \exp(E_1(\phi^{n+1}))) \theta_0^{n+1} \leq \exp(\delta t \gamma (\mathcal{G}\mu^{n+1}, \mu^{n+1}) + \ln(\tilde{r}^{n+1})) - \exp(E_1(\phi^{n+1})),$$

then $\theta_0^{n+1} \in \mathcal{W}$. Similar to BDF2 scheme, we need to choose θ_0^{n+1} satisfies following inequality (2.19)

$$(\tilde{r}^{n+1} - \exp(E_1(\phi^{n+1}))) \theta_0^{n+1} \leq \exp\left(\frac{2}{3} \delta t \gamma (\mathcal{G}\mu^{n+1}, \mu^{n+1}) + \ln(\tilde{r}^{n+1})\right) - \exp(E_1(\phi^{n+1})).$$

Denote $S = \exp(\delta t \gamma (\mathcal{G}\mu^{n+1}, \mu^{n+1}) + \ln(\tilde{r}^{n+1}))$ for BDF1 scheme and $S = \exp(\frac{2}{3} \delta t \gamma (\mathcal{G}\mu^{n+1}, \mu^{n+1}) + \ln(\tilde{r}^{n+1}))$ for BDF2 scheme, the next theorem summarizes the choice of θ_0^{n+1} .

THEOREM 2.1. *We choose θ_0^{n+1} in (2.15) as follows:*

1. If $\tilde{r}^{n+1} = \exp(E_1(\phi^{n+1}))$, we set $\theta_0^{n+1} = 0$.
2. If $\tilde{r}^{n+1} > \exp(E_1(\phi^{n+1}))$, we set $\theta_0^{n+1} = 0$.
3. If $\tilde{r}^{n+1} < \exp(E_1(\phi^{n+1}))$ and $S - \exp(E_1(\phi)) \geq 0$, we set $\theta_0^{n+1} = 0$.
4. If $\tilde{r}^{n+1} < \exp(E_1(\phi^{n+1}))$ and $S - \exp(E_1(\phi)) < 0$, we set $\theta_0^{n+1} = \frac{S - \exp(E_1(\phi^{n+1}))}{\tilde{r}^{n+1} - \exp(E_1(\phi^{n+1}))}$.

Then, (2.18) (resp. (2.19)) for BDF1 (resp. BDF2) scheme is satisfied in all cases above and $\theta_0^{n+1} \in \mathcal{W}$. Moreover, we have $r^{n+1} > 0$, and the scheme (2.8)-(2.15) with the above choice of θ_0^{n+1} satisfies unconditionally energy stability in the sense that:

First-order:

$$(2.20) \quad R_{R-ESAV-BDF1}^{n+1} - R_{R-ESAV-BDF1}^n \leq -\delta t(1 - \gamma) (\mathcal{G}\mu^{n+1}, \mu^{n+1}) \leq 0,$$

where $R_{R-ESAV-BDF1}^{n+1} = \frac{1}{2} (\mathcal{L}\phi^{n+1}, \phi^{n+1}) + \ln(r^{n+1})$;

Second-order:

$$(2.21) \quad R_{R-ESAV-BDF2}^{n+1} - R_{R-ESAV-BDF2}^n \leq -\delta t(1 - \gamma) (\mathcal{G}\mu^{n+1}, \mu^{n+1}) \leq 0,$$

where $R_{R-ESAV-BDF2}^{n+1} = \frac{1}{4} ((\mathcal{L}\phi^{n+1}, \phi^{n+1}) + (\mathcal{L}(2\phi^{n+1} - \phi^n), 2\phi^{n+1} - \phi^n)) + \frac{1}{2} (3 \ln(r^{n+1}) - \ln(r^n))$.
Furthermore, we have

$$(2.22) \quad r^{n+1} \leq \exp(E_1(\phi^{n+1})), \quad \forall n \geq 0.$$

Proof. It can be verified easily that the above choice of θ_0^{n+1} satisfies (2.18) (resp. (2.19)) for BDF1 (resp. BDF2) scheme in all cases such that $\theta_0^{n+1} \in \mathcal{W}$.

We can obtain that $\tilde{r}^{n+1} > 0$ from (2.10), and thanks to $\exp(E_1(\phi^{n+1})) > 0$, we have $r^{n+1} > 0$.

Taking the inner product of (2.8)-(2.9) with μ^{n+1} and $\frac{\phi^{n+1} - \phi^n}{\delta t}$ (resp. $\frac{3\phi^{n+1} - 4\phi^n + \phi^{n-1}}{2\delta t}$), respectively, combining them with the equation (2.10) and (2.16) (resp. (2.17)), we can derive the discrete energy dissipation law (2.20) (resp. (2.21)) for BDF1 (resp. BDF2) scheme.

For Cases 1-3, we have $\theta_0^{n+1} = 0$ so $r^{n+1} = E_1(\phi^{n+1})$. For Case 4, since

$$\theta_0^{n+1} = \frac{S - \exp(E_1(\phi^{n+1}))}{\bar{r}^{n+1} - \exp(E_1(\phi^{n+1}))} \in [0, 1]$$

and $\bar{r}^{n+1} < \exp(E_1(\phi^{n+1}))$, we can obtain that $r^{n+1} \leq \exp(E_1(\phi^{n+1}))$ from (2.15). The proof is complete. \square

Remark 2.1. To prevent the solution “blowing up” due to the rapid growth of exponential function, we can add a positive constant C to redefine the exponential SAV $r(t) = \exp\left(\frac{E_1(\phi)}{C}\right)$, which is similar to [20].

2.2. The application of R-ESAV-1 approach for gradient flows of multiple functions. We provide below the R-ESAV-1 approach for gradient flows of multiple functions by considering the following energy functional

$$(2.23) \quad E(\Phi) = \sum_{i,j=1}^m \frac{1}{2} d_{ij}(\phi_i, \mathcal{L}\phi_j) + E_1(\Phi),$$

where $\Phi = [\phi_1, \phi_2, \dots, \phi_m]^T$, \mathcal{L} is a self-adjoint linear positive definite operator, and the constant matrix $(d_{ij}), i, j = 1, \dots, m$ is symmetric positive definite. We set $W_i(\Phi) = \frac{\delta E_1(\Phi)}{\delta \phi_i}$, then the associated gradient flow is given by

$$(2.24) \quad \begin{cases} \frac{\partial \phi_i}{\partial t} = -\mathcal{G}\mu_i, \\ \mu_i = \frac{\delta E}{\delta \phi_i} = \sum_{j=1}^m d_{ij} \mathcal{L}\phi_j + Q_i(\Phi), \end{cases}$$

where \mathcal{G} is a nonnegative operator. Taking the inner products of (2.24) with μ_i and $\frac{\partial \phi_i}{\partial t}$ respectively, summing over i , and thanks to the self-adjoint of \mathcal{L} and $d_{ij} = d_{ji}$, we have the energy dissipation law as follows

$$(2.25) \quad \frac{d}{dt} E(\Phi) = \frac{d}{dt} \left\{ \frac{1}{2} \sum_{i,j=1}^m d_{ij}(\phi_i, \mathcal{L}\phi_j) + E_1(\Phi) \right\} = - \sum_{i=1}^m (\mathcal{G}\mu_i, \mu_i) \leq 0.$$

We construct numerical schemes for gradient flow of multiple functions by using R-ESAV-1 approach. Introducing an exponential SAV

$$(2.26) \quad r(t) = \exp(E_1(\Phi)),$$

then (2.24) can be rewritten as

$$(2.27) \quad \begin{cases} \frac{\partial \phi_i}{\partial t} = \mathcal{G}\mu_i, \\ \mu_i = \sum_{j=1}^m d_{ij} \mathcal{L}\phi_j + \frac{r}{\exp(E_1(\Phi))} Q_i(\Phi), \\ \frac{d \ln(r)}{dt} = \frac{r}{\exp(E_1(\Phi))} \sum_{i=1}^m \left(Q_i(\Phi), \frac{\partial \phi_i}{\partial t} \right). \end{cases}$$

Denote

$$U_i(r, \Phi) = \frac{r}{\exp(E_1(\Phi))} Q_i(\Phi),$$

then the system (2.27) can be simplified into

$$(2.28) \quad \begin{cases} \frac{\partial \phi_i}{\partial t} = \mathcal{G}\mu_i, \\ \mu_i = \sum_{j=1}^m d_{ij} \mathcal{L}\phi_j + U_i(r, \Phi), \\ \frac{d \ln(r)}{dt} = \sum_{i=1}^m \left(U_i(r, \Phi), \frac{\partial \phi_i}{\partial t} \right). \end{cases}$$

Taking the inner product of the first two equations in (2.28) with μ_i and $\frac{\partial \phi_i}{\partial t}$, respectively, combining them with the third equation in (2.28), and summing over i , we obtain the equivalent energy dissipation law

$$(2.29) \quad \frac{d}{dt} \left\{ \frac{1}{2} \sum_{i,j=1}^m d_{ij} (\phi_i, \mathcal{L}\phi_j) + \ln(r) \right\} = \frac{d}{dt} E(\Phi) = - \sum_{i=1}^m (\mathcal{G}\mu_i, \mu_i) \leq 0.$$

Next we can construct numerical scheme based on first version of R-ESAV approach and Crank-Nicolson formula (R-ESAV-1/CN) as follows.

Given $r^{n-1}, r^n, \Phi^{n-1}, \Phi^n$, we determine r^{n+1}, Φ^{n+1} via two steps as follows:

Step 1: Compute an intermediate solution $(\tilde{r}^{n+1}, \Phi^{n+1})$ by using the ESAV-1 approach:

$$(2.30) \quad \frac{\phi_i^{n+1} - \phi_i^n}{\delta t} = -\mathcal{G}\mu_i^{n+\frac{1}{2}},$$

$$(2.31) \quad \mu_i^{n+\frac{1}{2}} = \sum_{j=1}^m d_{ij} \mathcal{L}\phi_j^{n+\frac{1}{2}} + U_i(r^{*,n+\frac{1}{2}}, \Phi^{*,n+\frac{1}{2}}),$$

$$(2.32) \quad \frac{\ln(\tilde{r}^{n+1}) - \ln(r^n)}{\delta t} = \sum_{i=1}^m \left(U_i(r^{*,n+\frac{1}{2}}, \Phi^{*,n+\frac{1}{2}}), \frac{\phi_i^{n+1} - \phi_i^n}{\delta t} \right),$$

where $g^{n+\frac{1}{2}} = \frac{g^{n+1} + g^n}{2}$ and $g^{*,n+\frac{1}{2}}$ can be any second-order explicit approximation of $g(t^{n+1/2})$, such as $g^{*,n+\frac{1}{2}} = \frac{3}{2}g^n - \frac{1}{2}g^{n-1}$.

Step 2: Update r^{n+1} via relaxation factor as follows:

$$(2.33) \quad r^{n+1} = \theta_0^{n+1} \tilde{r}^{n+1} + (1 - \theta_0^{n+1}) \exp(E_1(\Phi^{n+1})), \quad \theta_0^{n+1} \in \mathcal{W},$$

where, \mathcal{W} is a set defined as follows:

$$(2.34) \quad \mathcal{W} = \left\{ \theta \in [0, 1] \text{ s.t. } \ln(r^{n+1}) - \ln(\tilde{r}^{n+1}) \leq \delta t \gamma \sum_{i=1}^m \left(\mathcal{G}\mu_i^{n+\frac{1}{2}}, \mu_i^{n+\frac{1}{2}} \right) \right\},$$

with $\gamma \in [0, 1]$ is a adjustable parameter.

Inserting (2.33) into the inequality of (2.34), we observe that if we choose θ_0^{n+1} satisfies following condition

$$(2.35) \quad (\tilde{r}^{n+1} - \exp(E_1(\Phi^{n+1}))) \theta_0^{n+1} \leq \exp \left(\delta t \gamma \sum_{i=1}^m \left(\mathcal{G}\mu_i^{n+\frac{1}{2}}, \mu_i^{n+\frac{1}{2}} \right) + \ln(\tilde{r}^{n+1}) \right) - \exp(E_1(\Phi^{n+1})),$$

then $\theta_0^{n+1} \in \mathcal{W}$. Denote $S = \exp \left(\delta t \gamma \sum_{i=1}^m \left(\mathcal{G}\mu_i^{n+\frac{1}{2}}, \mu_i^{n+\frac{1}{2}} \right) + \ln(\tilde{r}^{n+1}) \right)$, then we can choose θ_0^{n+1} according to Theorem 2.1 and the scheme (2.30)-(2.33) satisfies the unconditional energy stability

in the sense that

$$(2.36) \quad R_{R-ESAV-CN}^{n+1} - R_{R-ESAV-CN}^n \leq -\delta t(1-\gamma) \sum_{i=1}^m \left(\mathcal{G} \mu_i^{n+\frac{1}{2}}, \mu_i^{n+\frac{1}{2}} \right) \leq 0,$$

where $R_{R-ESAV-CN}^{n+1} = \frac{1}{2} \sum_{i,j=1}^m d_{ij} (\phi_i^{n+1}, \mathcal{L} \phi_j^{n+1}) + \ln(r^{n+1})$.

2.3. Extension to the multiple ESAV-1 approach. In this subsection, we present how to construct relaxed multiple ESAV-1 (R-MESAV-1) schemes for gradient flow, where the model may include disparate terms such that original schemes with only one SAV has limitation on describing the different disparate evolution processes and may require overly small time steps to obtain accurate numerical solution [4].

Without losing generality, we study gradient flow with two disparate nonlinear terms as follows and it can be easily extended to more than two disparate nonlinear terms

$$(2.37) \quad \begin{cases} \frac{\partial \phi}{\partial t} = -\mathcal{G}\mu, \\ \mu = \mathcal{L}\phi + F_1'(\phi) + F_2'(\phi), \end{cases}$$

where \mathcal{L} is a self-adjoint linear elliptic operator, $F_1(\phi), F_2(\phi)$ are nonlinear potential function, \mathcal{G} is a linear positive definite operator. The system (2.37) satisfies the following energy dissipation law

$$(2.38) \quad \frac{dE(\phi)}{dt} = -(\mathcal{G}\mu, \mu),$$

where the total energy is

$$(2.39) \quad E(\phi) = \frac{1}{2}(\mathcal{L}\phi, \phi) + \int_{\Omega} F_1(\phi) d\mathbf{x} + \int_{\Omega} F_2(\phi) d\mathbf{x}.$$

We first consider relaxed MESAV approach based on first ESAV approach. Setting $E_1(\phi) = \int_{\Omega} F_1(\phi) d\mathbf{x}$, $E_2(\phi) = \int_{\Omega} F_2(\phi) d\mathbf{x}$ and introducing two SAVs $r_1(t) = \exp(E_1(\phi))$, $r_2(t) = \exp(E_2(\phi))$, we can rewrite the system (2.37) as

$$(2.40) \quad \begin{cases} \frac{\partial \phi}{\partial t} = -\mathcal{G}\mu, \\ \mu = \mathcal{L}\phi + \frac{r_1(t)}{\exp(E_1(\phi))} F_1'(\phi) + \frac{r_2(t)}{\exp(E_2(\phi))} F_2'(\phi), \\ \frac{dr_1(t)}{dt} = \frac{r_1^2}{\exp(E_1(\phi))} (F_1'(\phi), \phi_t), \\ \frac{dr_2(t)}{dt} = \frac{r_2^2}{\exp(E_2(\phi))} (F_2'(\phi), \phi_t). \end{cases}$$

Denote $U_1(r_1, \phi) = \frac{r_1}{\exp(E_1(\phi))} F_1'(\phi)$ and $U_2(r_2, \phi) = \frac{r_2}{\exp(E_2(\phi))} F_2'(\phi)$, then (2.40) can be transformed as

$$(2.41) \quad \begin{cases} \frac{\partial \phi}{\partial t} = -\mathcal{G}\mu, \\ \mu = \mathcal{L}\phi + U_1(r_1, \phi) + U_2(r_2, \phi), \\ \frac{d \ln(r_1)}{dt} = (U_1(r_1, \phi), \phi_t), \\ \frac{d \ln(r_2)}{dt} = (U_2(r_2, \phi), \phi_t). \end{cases}$$

Then we can construct R-MESAV-1/CN schemes inspired by the idea of relaxation factor. Given $\phi^{n-1}, \phi^n, r_1^{n-1}, r_1^n, r_2^{n-1}, r_2^n$, we determine $\phi^{n+1}, r_1^{n+1}, r_2^{n+1}$ via two steps as follows:

Step 1: Compute an intermediate solution $(\phi^{n+1}, \tilde{r}_1^{n+1}, \tilde{r}_2^{n+1})$ by using the MESAV approach:

$$(2.42) \quad \frac{\phi^{n+1} - \phi^n}{\delta t} = -\mathcal{G}\mu^{n+\frac{1}{2}},$$

$$(2.43) \quad \mu^{n+\frac{1}{2}} = \mathcal{L}\phi^{n+\frac{1}{2}} + U_1 \left(r_1^{*,n+\frac{1}{2}}, \phi^{*,n+\frac{1}{2}} \right) + U_2 \left(r_2^{*,n+\frac{1}{2}}, \phi^{*,n+\frac{1}{2}} \right),$$

$$(2.44) \quad \frac{\ln(\tilde{r}_1^{n+1}) - \ln(r_1^n)}{\delta t} = \left(U_1 \left(r_1^{*,n+\frac{1}{2}}, \phi^{*,n+\frac{1}{2}} \right), \frac{\phi^{n+1} - \phi^n}{\delta t} \right),$$

$$(2.45) \quad \frac{\ln(\tilde{r}_2^{n+1}) - \ln(r_2^n)}{\delta t} = \left(U_2 \left(r_2^{*,n+\frac{1}{2}}, \phi^{*,n+\frac{1}{2}} \right), \frac{\phi^{n+1} - \phi^n}{\delta t} \right).$$

Step 2: Update the SAVs r_1^{n+1}, r_2^{n+1} via relaxation factor as follows:

$$(2.46) \quad \begin{aligned} r_1^{n+1} &= \theta_0^{n+1} \tilde{r}_1^{n+1} + (1 - \theta_0^{n+1}) \exp(E_1(\phi^{n+1})), & \theta_0^{n+1} \in \mathcal{W}, \\ r_2^{n+1} &= \theta_0^{n+1} \tilde{r}_2^{n+1} + (1 - \theta_0^{n+1}) \exp(E_2(\phi^{n+1})), & \theta_0^{n+1} \in \mathcal{W}, \end{aligned}$$

where \mathcal{W} is a set defined as follows:

$$(2.47) \quad \mathcal{W} = \left\{ \theta \in [0, 1] \text{ s.t. } \ln(r_1^{n+1}) + \ln(r_2^{n+1}) - \ln(\tilde{r}_1^{n+1}) - \ln(\tilde{r}_2^{n+1}) \leq \delta t \gamma \left(\mathcal{G}\mu^{n+\frac{1}{2}}, \mu^{n+\frac{1}{2}} \right) \right\}$$

with $\gamma \in [0, 1]$ is an adjustable parameter.

We explain below how to choose θ_0^{n+1} . Plugging (2.46) into (2.47), we derive that if we choose θ_0^{n+1} such that

$$(2.48) \quad \begin{aligned} & [(\tilde{r}_1^{n+1} - \exp(E_1(\phi^{n+1}))) \theta_0^{n+1} + \exp(E_1(\phi^{n+1}))] [(\tilde{r}_2^{n+1} - \exp(E_2(\phi^{n+1}))) \theta_0^{n+1} + \exp(E_2(\phi^{n+1}))] \\ & \leq \exp \left(\delta t \gamma \left(\mathcal{G}\mu^{n+\frac{1}{2}}, \mu^{n+\frac{1}{2}} \right) + \ln(\tilde{r}_1^{n+1}) + \ln(\tilde{r}_2^{n+1}) \right), \end{aligned}$$

then $\theta_0^{n+1} \in \mathcal{W}$. And θ_0^{n+1} can be regarded as a solution of the optimization problem as follows

$$(2.49) \quad \theta_0^{n+1} = \min_{\theta \in [0, 1]} \theta, \quad \text{s.t. } f(\theta) = a_1 a_2 \theta^2 + (a_1 b_2 + a_2 b_1) \theta + b_1 b_2 - c \leq 0,$$

where the coefficients are

$$\begin{aligned} a_1 &= \tilde{r}_1^{n+1} - \exp(E_1(\phi^{n+1})), & b_1 &= \exp(E_1(\phi^{n+1})), \\ a_2 &= \tilde{r}_2^{n+1} - \exp(E_2(\phi^{n+1})), & b_2 &= \exp(E_2(\phi^{n+1})), \\ c &= \exp \left(\delta t \gamma \left(\mathcal{G}\mu^{n+\frac{1}{2}}, \mu^{n+\frac{1}{2}} \right) + \ln(\tilde{r}_1^{n+1}) + \ln(\tilde{r}_2^{n+1}) \right). \end{aligned}$$

Denote

$$\begin{aligned} \theta_1 &= \frac{-(a_1 b_2 + a_2 b_1) - \sqrt{(a_1 b_2 + a_2 b_1)^2 - 4a_1 a_2 (b_1 b_2 - c)}}{2a_1 a_2}, \\ \theta_2 &= \frac{-(a_1 b_2 + a_2 b_1) + \sqrt{(a_1 b_2 + a_2 b_1)^2 - 4a_1 a_2 (b_1 b_2 - c)}}{2a_1 a_2}, \end{aligned}$$

and the next theorem summarizes the choice of θ_0^{n+1} .

THEOREM 2.2. *We choose θ_0^{n+1} in (2.46) as follows:*

1. If $a_1 = 0$ and $a_2 = 0$, we set $\theta_0^{n+1} = 0$.
2. If $a_1 > 0$ and $a_2 > 0$, we set $\theta_0^{n+1} = 0$.

3. If $a_1 < 0$ and $a_2 < 0$, we set $\theta_0^{n+1} = \max\{0, \theta_1\}$.
4. If $a_1 a_2 < 0$ and $b_1 b_2 - c \leq 0$, we set $\theta_0^{n+1} = 0$.
5. If $a_1 a_2 < 0$ and $b_1 b_2 - c > 0$, we set $\theta_0^{n+1} = \theta_1$.
6. If $a_1 a_2 = 0$ and $a_1 b_2 + a_2 b_1 > 0$, we set $\theta_0^{n+1} = 0$.
7. If $a_1 a_2 = 0$ and $a_1 b_2 + a_2 b_1 < 0$, we set $\theta_0^{n+1} = \max\left\{0, \frac{c-b_1 b_2}{a_1 b_2 + a_2 b_1}\right\}$.

Then, (2.48) for scheme (2.42)-(2.46) is satisfied in all cases above and $\theta_0^{n+1} \in \mathcal{W}$. Moreover, we have $r_1^{n+1} > 0$, $r_2^{n+1} > 0$, and the scheme (2.42)-(2.46) with the above choice of θ_0^{n+1} is unconditionally energy stable in the sense that:

$$(2.50) \quad R_{R-MESAV-CN}^{n+1} - R_{R-MESAV-CN}^n \leq -\delta t(1-\gamma) (\mathcal{G}\mu^{n+1}, \mu^{n+1}) \leq 0,$$

where $R_{R-MESAV-CN}^{n+1} = \frac{1}{2} (\mathcal{L}\phi^{n+1}, \phi^{n+1}) + \ln(r_1^{n+1}) + \ln(r_2^{n+1})$.

Proof. We find optimal relaxation θ_0^{n+1} by discussing the coefficient of (2.49) case by case.

- If $a_1 = 0$ and $a_2 = 0$, we have $\theta_0^{n+1} = 0$ obviously.
- If $a_1 a_2 \neq 0$, notice that

$$f(1) = \tilde{r}_1^{n+1} \tilde{r}_2^{n+1} - \exp\left(\delta t \gamma (\mathcal{G}\mu^{n+\frac{1}{2}}, \mu^{n+\frac{1}{2}}) + \ln(\tilde{r}_1^{n+1}) + \ln(\tilde{r}_2^{n+1})\right) \leq 0,$$

we have $1 \in \mathcal{W}$ which means $\mathcal{W} \neq \emptyset$.

- If $a_1 a_2 > 0$, and thanks to $f(1) \leq 0$, we have $\theta_0^{n+1} = \max\{0, \theta_1\}$, then we can easily derive Case 2, 3.
- If $a_1 a_2 < 0$, and $f(0) = b_1 b_2 - c \leq 0$, we have $\theta_0^{n+1} = 0$.
- If $a_1 a_2 < 0$, and $f(0) = b_1 b_2 - c > 0$, $f(1) \leq 0$, we have $\theta_0^{n+1} = \max\{\theta_1, \theta_2\}$. And since $\theta_1 \geq \theta_2$, then $\theta_0^{n+1} = \theta_1$.
- If $a_1 a_2 = 0$, and $a_1 b_2 + a_2 b_1 > 0$, thanks to $f(1) \leq 0$, we have $\theta_0^{n+1} = 0$.
- If $a_1 a_2 = 0$, and $a_1 b_2 + a_2 b_1 < 0$, since $f(1) \leq 0$, then we have $\theta_0^{n+1} = \max\left\{0, \frac{c-b_1 b_2}{a_1 b_2 + a_2 b_1}\right\}$.

We derive from (2.44)-(2.45) that $\tilde{r}_1^{n+1} > 0$, $\tilde{r}_2^{n+1} > 0$, and thanks to $\exp(E_1(\phi^{n+1})) > 0$, $\exp(E_2(\phi^{n+1})) > 0$, we have $r_1^{n+1} > 0$, $r_2^{n+1} > 0$.

Taking the inner product of (2.42)-(2.43) with μ^{n+1} and $\frac{\phi^{n+1} - \phi^n}{\delta t}$, respectively, combining them with the equation (2.44)-(2.45) and (2.47), we can obtain the desired result (2.50). \square

3. The second version of relaxed exponential SAV approach. Inspired by the total energy based on exponential SAV approach in [21], we construct the second version of relaxed exponential SAV approach(R-ESAV-2) for dissipative system in this section.

3.1. The R-ESAV-2 approach for dissipative system. More generally, we consider dissipative system

$$(3.1) \quad \frac{\partial \phi}{\partial t} + \mathcal{A}\phi + g(\phi) = 0,$$

where \mathcal{A} is a positive operator and $g(\phi)$ is a semi-linear or quasi-linear operator. Assume it satisfies the following energy dissipation law

$$(3.2) \quad \frac{dE(\phi)}{dt} = -\mathcal{K}(\phi),$$

where $E(\phi) > -C_0$ is a free energy and $\mathcal{K}(\phi) > 0$ for all ϕ . Introducing a SAV $R(t) = \exp(E(\phi))$, we transform the equation (3.1) into the equivalent system as follows

$$(3.3) \quad \begin{cases} \frac{\partial \phi}{\partial t} + \mathcal{A}(\phi) + V(\xi)g(\phi) = 0, \\ \frac{dR(t)}{dt} = -R(t)\mathcal{K}(\phi), \\ \xi = \frac{R(t)}{\exp(E(\phi))}, \end{cases}$$

where $V(\xi)$ is a function related to ξ and $V(\xi) \equiv 1$ at a continuous level.

Then we can construct R-ESAV-2/BDF k ($1 \leq k \leq 6$) schemes inspired by the idea of relaxation factor.

Given $R^{n-k}, \dots, R^n, \phi^{n-k}, \dots, \phi^n$, we determine R^{n+1}, ϕ^{n+1} via two steps as follows:

Step 1: Compute an intermediate solution $(\tilde{R}^{n+1}, \phi^{n+1})$ by using the ESAV approach:

$$(3.4) \quad \frac{\alpha_k \phi^{n+1} - A_k(\phi^n)}{\delta t} + \mathcal{A}\phi^{n+1} + V_k(\xi^{n+1})g(B_k(\phi^n)) = 0,$$

$$(3.5) \quad \frac{1}{\delta t} (\tilde{R}^{n+1} - R^n) = -\tilde{R}^{n+1}\mathcal{K}(B_k(\phi^n)),$$

$$(3.6) \quad \xi^{n+1} = \frac{\tilde{R}^{n+1}}{\exp(E(B_k(\phi^n)))},$$

where α_k, A_k and B_k are defined as above and $V_k(\xi^{n+1})$ for k th-order ($1 \leq k \leq 4$) scheme are following:

First-order: $V_1(\xi^{n+1}) = \xi^{n+1}$;

Second-order: $V_2(\xi^{n+1}) = \xi^{n+1}(2 - \xi^{n+1})$;

Third-order: $V_3(\xi^{n+1}) = \xi^{n+1}(3 - 3\xi^{n+1} + (\xi^{n+1})^2)$;

Forth-order: $V_4(\xi^{n+1}) = \xi^{n+1}(2 - \xi^{n+1})(2 - 2\xi^{n+1} + (\xi^{n+1})^2)$.

Step 2: Update the SAV R^{n+1} via relaxation factor as follows:

$$(3.7) \quad R^{n+1} = \theta_0^{n+1}\tilde{R}^{n+1} + (1 - \theta_0^{n+1})\exp(E(\phi^{n+1})), \quad \theta_0^{n+1} \in \mathcal{W},$$

where

$$(3.8) \quad \mathcal{W} = \left\{ \theta \in [0, 1] \text{ s.t. } \frac{R^{n+1} - \tilde{R}^{n+1}}{\delta t} = -\gamma^{n+1}\tilde{R}^{n+1}\mathcal{K}(\phi^{n+1}) + \tilde{R}^{n+1}\mathcal{K}(B_k(\phi^n)) \right\},$$

and $\gamma^{n+1} \geq 0$ is to be determined such that the set \mathcal{W} is not empty.

Then we describe how to choose θ_0^{n+1} and γ^{n+1} . Insertting (3.7) into the equality of the set (3.8), we derive that if we choose θ_0^{n+1} and γ^{n+1} such that

$$(3.9) \quad \left(\tilde{R}^{n+1} - \exp(E(\phi^{n+1})) \right) \theta_0^{n+1} = \tilde{R}^{n+1} - \exp(E(\phi^{n+1})) - \delta t \gamma^{n+1} \tilde{R}^{n+1} \mathcal{K}(\phi^{n+1}) + \delta t \tilde{R}^{n+1} \mathcal{K}(B_k(\phi^n)),$$

then, $\theta_0^{n+1} \in \mathcal{W}$. The summation of the choice of θ_0^{n+1} and γ^{n+1} are provided in next theorem.

THEOREM 3.1. *The choice of θ_0^{n+1} in (3.7) and γ^{n+1} in (3.8) are shown as follows:*

1. If $\tilde{R}^{n+1} = \exp(E(\phi^{n+1}))$, we set $\theta_0^{n+1} = 0$ and $\gamma^{n+1} = \frac{\mathcal{K}(B_k(\phi^n))}{\mathcal{K}(\phi^{n+1})}$.
2. If $\tilde{R}^{n+1} > \exp(E(\phi^{n+1}))$, we set $\theta_0^{n+1} = 0$ and

$$(3.10) \quad \gamma^{n+1} = \frac{\tilde{R}^{n+1} - \exp(E(\phi^{n+1}))}{\delta t \tilde{R}^{n+1} \mathcal{K}(\phi^{n+1})} + \frac{\mathcal{K}(B_k(\phi^n))}{\mathcal{K}(\phi^{n+1})}.$$

3. If $\tilde{R}^{n+1} < \exp(E(\phi^{n+1}))$ and $\tilde{R}^{n+1} - \exp(E(\phi^{n+1})) + \delta t \tilde{R}^{n+1} \mathcal{K}(B_k(\phi^n)) \geq 0$, we set $\theta_0^{n+1} = 0$ and γ^{n+1} the same as (3.10).
4. If $\tilde{R}^{n+1} < \exp(E(\phi^{n+1}))$ and $\tilde{R}^{n+1} - \exp(E(\phi^{n+1})) + \delta t \tilde{R}^{n+1} \mathcal{K}(B_k(\phi^n)) < 0$, we set $\theta_0^{n+1} = 1 - \frac{\delta t \tilde{R}^{n+1} \mathcal{K}(B_k(\phi^n))}{\exp(E(\phi^{n+1})) - \tilde{R}^{n+1}}$ and $\gamma^{n+1} = 0$.

Then, (3.9) is satisfied in all cases above and $\theta_0^{n+1} \in \mathcal{W}$. Moreover, we have $R^{n+1} > 0$, $\xi_k^{n+1} > 0$, and the scheme (3.4)-(3.7) with the above choice of θ_0^{n+1} and γ^{n+1} satisfies unconditionally energy stability in the sense that

$$(3.11) \quad R^{n+1} - R^n = -\delta t \gamma^{n+1} \tilde{R}^{n+1} \mathcal{K}(\phi^{n+1}) \leq 0,$$

and more importantly we have

$$(3.12) \quad \ln(R^{n+1}) - \ln(R^n) \leq 0.$$

Furthermore, we have

$$(3.13) \quad R^{n+1} \leq \exp(E(\phi^{n+1})), \quad \forall n \geq 0.$$

Proof. It can be verified easily that the above choice of θ_0^{n+1} and γ^{n+1} satisfies (3.9) in all cases such that $\theta_0^{n+1} \in \mathcal{W}$.

Since $R^0 > 0$. It follows from (3.5) that

$$(3.14) \quad \tilde{R}^1 = \frac{R^0}{1 + \delta t \mathcal{K}(B_k(\phi^0))} > 0.$$

Then we derive from (3.6) that $\xi_k^1 > 0$, and we derive from (3.7) that $R^1 > 0$. Therefore, it is easy to obtain $\xi_k^{n+1} > 0$ and $R^{n+1} > 0$ by induction method.

Then we obtain (3.11) by combining (3.5) and (3.8).

For Cases 1-3, it can obtain that $\theta_0^{n+1} = 0$, then we have $R^{n+1} = \exp(E(\phi^{n+1}))$. For Case 4, thanks to $\theta_0^{n+1} = 1 - \frac{\delta t \tilde{R}^{n+1} \mathcal{K}(B_k(\phi^n))}{\exp(E(\phi^{n+1})) - \tilde{R}^{n+1}} \in (0, 1]$ and $\tilde{R}^{n+1} < \exp(E(\phi^{n+1}))$, we derive that $R^{n+1} \leq \exp(E(\phi^{n+1}))$ from (3.7). \square

Remark 3.1. As a further extension, firstly, we can also construct numerical schemes for gradient flows of multiple functions (2.24) by using the R-ESAV-2 approach, and $\theta_0^{n+1}, \gamma^{n+1}$ can be chosen similarly according to Theorem 3.1. Secondly, the R-ESAV-2 approach can be also extended to multiple ESAV form based on gradient flow with two disparate nonlinear terms (2.37). Setting $E_1(\phi) = \frac{1}{2}(\mathcal{L}\phi, \phi) + \int_{\Omega} F_1(\phi) d\mathbf{x}$, $E_2(\phi) = \int_{\Omega} F_2(\phi) d\mathbf{x}$ and introducing two SAVs $R_1(t) = \exp(E_1(\phi))$, $R_2(t) = \exp(E_2(\phi))$, we can rewrite the equation (2.37) as

$$(3.15) \quad \begin{cases} \frac{\partial \phi}{\partial t} = -\mathcal{G}\mu, \\ \mu = \mathcal{L}\phi + V(\xi_1)F_1'(\phi) + V(\xi_2)F_2'(\phi), \\ \frac{d \ln(R_1(t))}{dt} = -\left(\mathcal{G} \frac{\delta E_1}{\delta \phi}, \mu\right), \\ \frac{d \ln(R_2(t))}{dt} = -\left(\mathcal{G} \frac{\delta E_2}{\delta \phi}, \mu\right), \\ \xi_1 = \frac{R_1(t)}{\exp(E_1(\Phi))}, \quad \xi_2 = \frac{R_2(t)}{\exp(E_2(\Phi))}. \end{cases}$$

The forms of the third and fourth energy equations of (3.15) are different from that in (3.3). Then we can construct BDFk numerical schemes for above system. And we can choose θ_0^{n+1} according to Theorem 2.2 if we set $0 \leq \gamma \leq \frac{(\mathcal{G}\mu(B_k(\phi^n)), \mu(B_k(\phi^n)))}{(\mathcal{G}\mu^{n+1}, \mu^{n+1})}$.

3.2. The fully decoupled R-ESAV-2 approach for Navier-Stokes equation. In this subsection, we consider the fully decoupled R-ESAV-2 approach for the following incompressible Navier-Stokes equation, which is a classic dissipative system

$$(3.16) \quad \begin{cases} \frac{\partial \mathbf{u}}{\partial t} - \nu \Delta \mathbf{u} + (\mathbf{u} \cdot \nabla) \mathbf{u} + \nabla p = \mathbf{f} & \text{in } \Omega \times \mathcal{T}, \\ \nabla \cdot \mathbf{u} = 0 & \text{in } \Omega \times \mathcal{T}, \\ \mathbf{u} = \mathbf{0} & \text{on } \partial\Omega \times \mathcal{T}, \end{cases}$$

where Ω is an open bounded domain in $\mathbb{R}^d (d = 2, 3)$ with a sufficiently smooth boundary $\partial\Omega$, $\mathcal{T} = (0, T]$, \mathbf{u}, p are the unknown velocity and pressure respectively, \mathbf{f} represents an external body force, $\nu > 0$ is the viscosity coefficient and \mathbf{n} is the unit outward normal of the domain Ω . The system (3.16) satisfies the following law

$$(3.17) \quad \frac{d}{dt} E(\mathbf{u}) = -\nu \|\nabla \mathbf{u}\|^2 + (\mathbf{f}, \mathbf{u}),$$

where $E(\mathbf{u}) = \frac{1}{2} \|\mathbf{u}\|^2$ is the total energy.

Then we can consider the R-ESAV-2 approach for Navier-Stokes equation (3.16).

Introduce an exponential SAV $R(t) = \exp(E(\mathbf{u}))$, then we can rewrite the governing system (3.16) into the equivalent form as follows

$$(3.18) \quad \begin{cases} \frac{\partial \mathbf{u}}{\partial t} + V(\xi)(\mathbf{u} \cdot \nabla) \mathbf{u} - \nu \Delta \mathbf{u} + \nabla p = \mathbf{f}, \\ \nabla \cdot \mathbf{u} = 0, \\ \frac{dR(t)}{dt} = -\nu R(t) \|\nabla \mathbf{u}\|^2 + R(t)(\mathbf{f}, \mathbf{u}), \\ \xi = \frac{R(t)}{\exp(E(\mathbf{u}))}. \end{cases}$$

Next, we construct two BDF k schemes for (3.18). First one is based on pressure correction approach.

Scheme I: Given $\mathbf{u}^{n-k}, \dots, \mathbf{u}^n, p^{n-k}, \dots, p^n, r^{n-k}, \dots, r^n$, we solve $\mathbf{u}^{n+1}, p^{n+1}, r^{n+1}$ via four steps as follows:

Step 1: Determine solution \tilde{R}^{n+1} and compute ξ^{n+1} :

$$(3.19) \quad \frac{\tilde{R}^{n+1} - R^n}{\delta t} = -\nu \tilde{R}^{n+1} \|\nabla B_k(\mathbf{u}^n)\|^2 + \tilde{R}^{n+1}(\mathbf{f}^{n+1}, B_k(\mathbf{u}^n)),$$

$$(3.20) \quad \xi^{n+1} = \frac{\tilde{R}^{n+1}}{\exp(E(B_k(\mathbf{u}^n)))}.$$

Step 2: Compute an intermediate solution $\tilde{\mathbf{u}}^{n+1}$:

$$(3.21) \quad \frac{\alpha_k \tilde{\mathbf{u}}^{n+1} - A_k(\mathbf{u}^n)}{\delta t} + V(\xi^{n+1})(B_k(\mathbf{u}^n) \cdot \nabla) B_k(\mathbf{u}^n) - \nu \Delta \tilde{\mathbf{u}}^{n+1} + \nabla \hat{B}_k(p^n) = \mathbf{f}^{n+1},$$

$$(3.22) \quad \tilde{\mathbf{u}}^{n+1}|_{\partial\Omega} = 0.$$

Step 3: Solve solution $(\mathbf{u}^{n+1}, p^{n+1})$:

$$(3.23) \quad \frac{\alpha_k \mathbf{u}^{n+1} - \alpha_k \tilde{\mathbf{u}}^{n+1}}{\delta t} + \nabla (p^{n+1} - \hat{B}_k(p^n)) = 0,$$

$$(3.24) \quad \nabla \cdot \mathbf{u}^{n+1} = 0,$$

$$(3.25) \quad \mathbf{u}^{n+1} \cdot \mathbf{n}|_{\partial\Omega} = 0,$$

where operator $\hat{B}_1 = B_1$ for BDF1 scheme and $\hat{B}_k = B_{k-1}$ for BDF k ($k \geq 2$) scheme.

Step 4: Update the SAV R^{n+1} via relaxation factor as follows:

$$(3.26) \quad R^{n+1} = \theta_0^{n+1} \tilde{R}^{n+1} + (1 - \theta_0^{n+1}) \exp(E(\mathbf{u}^{n+1})), \quad \theta_0^{n+1} \in \mathcal{W},$$

where, \mathcal{W} is a set defined as follows:

$$(3.27) \quad \mathcal{W} = \left\{ \theta \in [0, 1] \text{ s.t. } \frac{R^{n+1} - \tilde{R}^{n+1}}{\delta t} = -\gamma^{n+1} \nu \tilde{R}^{n+1} \|\nabla \mathbf{u}^{n+1}\|^2 + \nu \tilde{R}^{n+1} \|\nabla B_k(\mathbf{u}^n)\|^2 \right\},$$

with $\gamma^{n+1} \geq 0$ to be determined such that \mathcal{W} is not empty.

Inspired by projection method in [29, 11], we can construct the following fully decoupled R-ESAV-2 scheme:

Scheme II: Given $\mathbf{u}^{n-k}, \dots, \mathbf{u}^n, p^{n-k}, \dots, p^n, r^{n-k}, \dots, r^n$, we determine $\mathbf{u}^{n+1}, p^{n+1}, r^{n+1}$ via two steps as follows:

Step 1: Solve solution $(\mathbf{u}^{n+1}, p^{n+1}, \tilde{R}^{n+1})$:

$$(3.28) \quad \frac{\alpha_k \mathbf{u}^{n+1} - A_k(\mathbf{u}^n)}{\delta t} - \nu \Delta \mathbf{u}^{n+1} + V(\xi^{n+1})(B_k(\mathbf{u}^n) \cdot \nabla) B_k(\mathbf{u}^n) + \nabla B_k(p^n) = \mathbf{f}^{n+1},$$

$$(3.29) \quad \frac{\tilde{R}^{n+1} - R^n}{\delta t} = -\nu \tilde{R}^{n+1} \|\nabla B_k(\mathbf{u}^n)\|^2 + \tilde{R}^{n+1}(\mathbf{f}^{n+1}, B_k(\mathbf{u}^n)),$$

$$(3.30) \quad \xi^{n+1} = \frac{\tilde{R}^{n+1}}{\exp(E(B_k(\mathbf{u}^n)))},$$

$$(3.31) \quad (\nabla p^{n+1}, \nabla q) = (\mathbf{f}^{n+1} - (\mathbf{u}^{n+1} \cdot \nabla) \mathbf{u}^{n+1} - \nu \nabla \times \nabla \times \mathbf{u}^{n+1}, \nabla q) \\ = (\mathbf{f}^{n+1} - (\mathbf{u}^{n+1} \cdot \nabla) \mathbf{u}^{n+1}, \nabla q) - \nu \int_{\partial \Omega} ((\nabla \times \mathbf{u}^{n+1}) \times \nabla q) \cdot \mathbf{n} ds,$$

where \mathbf{n} is the outward normal of $\partial \Omega$.

Step 2: Update the SAV R^{n+1} via relaxation factor as follows:

$$(3.32) \quad R^{n+1} = \theta_0^{n+1} \tilde{R}^{n+1} + (1 - \theta_0^{n+1}) \exp(E(\mathbf{u}^{n+1})), \quad \theta_0^{n+1} \in \mathcal{W},$$

where, \mathcal{W} is a set defined as follows:

$$(3.33) \quad \mathcal{W} = \left\{ \theta \in [0, 1] \text{ s.t. } \frac{R^{n+1} - \tilde{R}^{n+1}}{\delta t} = -\gamma^{n+1} \nu \tilde{R}^{n+1} \|\nabla \mathbf{u}^{n+1}\|^2 + \nu \tilde{R}^{n+1} \|\nabla B_k(\mathbf{u}^n)\|^2 \right\},$$

and $\gamma^{n+1} \geq 0$ is to be determined such that the set \mathcal{W} is not empty.

Remark 3.2. In the case of periodic boundary condition, the operators $\nabla, \nabla \cdot$ and Δ^{-1} can commute with each other by defining them in the Fourier space. In the absence of \mathbf{f} , taking the divergence on both sides of first equation of (3.16), we obtain

$$(3.34) \quad -\Delta p = \nabla \cdot (\mathbf{u} \cdot \nabla \mathbf{u}),$$

Then the first equation of (3.16) can be rewritten as

$$(3.35) \quad \frac{\partial \mathbf{u}}{\partial t} - \nu \Delta \mathbf{u} - \mathbf{J}(\mathbf{u} \cdot \nabla \mathbf{u}) = \mathbf{0},$$

where \mathbf{J} is defined by

$$(3.36) \quad \mathbf{J}\mathbf{v} := \nabla \times \nabla \times \Delta^{-1} \mathbf{v} \quad \forall \mathbf{v} \in \mathbf{L}_0^2(\Omega).$$

Moreover, in addition to (3.17), the system (3.16) satisfies energy dissipation law as follows

$$(3.37) \quad \frac{1}{2} \frac{d}{dt} \|\nabla \mathbf{u}\|^2 = -\nu \|\Delta \mathbf{u}\|^2.$$

Thus, (3.28)-(3.31) can be replaced by

$$(3.38) \quad \frac{\alpha_k \mathbf{u}^{n+1} - A_k(\mathbf{u}^n)}{\delta t} - \nu \Delta \mathbf{u}^{n+1} - V(\xi^{n+1}) \mathbf{J}(B_k(\mathbf{u}^n) \cdot \nabla B_k(\mathbf{u}^n)) = \mathbf{0},$$

$$(3.39) \quad \frac{\tilde{R}^{n+1} - R^n}{\delta t} = -\nu \tilde{R}^{n+1} \|\Delta B_k(\mathbf{u}^n)\|^2,$$

$$(3.40) \quad \xi^{n+1} = \frac{\tilde{R}^{n+1}}{\exp(E(B_k(\mathbf{u}^n)))},$$

$$(3.41) \quad \Delta p^{n+1} = -\nabla \cdot (\mathbf{u}^{n+1} \cdot \nabla \mathbf{u}^{n+1}).$$

Setting $K(\mathbf{u}) = \nu \|\nabla \mathbf{u}\|^2$ or $K(\mathbf{u}) = \nu \|\Delta \mathbf{u}\|^2$, we can choose θ_0^{n+1} and γ^{n+1} in Scheme I and Scheme II according to Theorem 3.1. Similarly, above schemes satisfy energy dissipation law (3.11) and (3.12).

4. Numerical simulations. In this section, we demonstrate ample numerical results to verify that the constructed R-ESAV-1 and R-ESAV-2 approaches are accurate and efficient. Besides, we also give detailed comparisons between the original ESAV schemes with the constructed R-ESAV schemes. We consider the numerical examples with periodic boundary condition and use the Fourier spectral method for spatial discretization in what follows unless explicitly given, and the dissipation rate parameter γ is set to 1 for the R-ESAV-1 schemes by default.

Example 1. We first consider the Allen-Cahn equation

$$(4.1) \quad \frac{\partial \phi}{\partial t} = \sigma_0 \Delta \phi + (1 - \phi^2) \phi.$$

(i) We give an exact solution

$$(4.2) \quad \phi(x, y, t) = \exp(\sin(\pi x) \sin(\pi y)) \sin(t),$$

and f is the external force satisfying (4.1). We set computational domain $\Omega = [0, 2]^2$ and the model parameter $\sigma_0 = 0.01^2$. For spatial discretization, we use Fourier mode $N^2 = 64^2$, so that compared with the time discretization error, the spatial discretization error is negligible.

The convergence rates of the L^2 error at $T = 1$ obtained by various schemes are presented in Fig. 1, where we can observe that

- (a) Numerical results are all consistent with the expected convergence rates;
- (b) The errors of R-ESAV-1 (resp. R-ESAV-2) schemes for BDF1 scheme are obviously smaller than that of ESAV-1 (resp. ESAV-2) schemes;
- (c) The improvement in the accuracy for the ESAV schemes with relaxation for higher-order schemes is not as notable as for first-order scheme.

We also demonstrate the evolution of relaxation factor θ_0^{n+1} obtained by R-ESAV-1/BDF2 and R-ESAV-2/BDF2 scheme with time step $\delta t = 1e - 3$ in Fig. 2. It can be obviously show that θ_0^{n+1} always takes the value zeros except at an initial time interval for R-ESAV-2/BDF2 scheme.

(ii) We choose the initial condition as

$$(4.3) \quad \phi(x, y) = \tanh \frac{1.5 + 1.2 \cos(6\lambda) - 2\pi\rho}{\sqrt{2\alpha}},$$

$$\lambda = \arctan \frac{y - 0.5}{x - 0.5}, \quad \rho = \sqrt{\left(x - \frac{1}{2}\right)^2 + \left(y - \frac{1}{2}\right)^2},$$

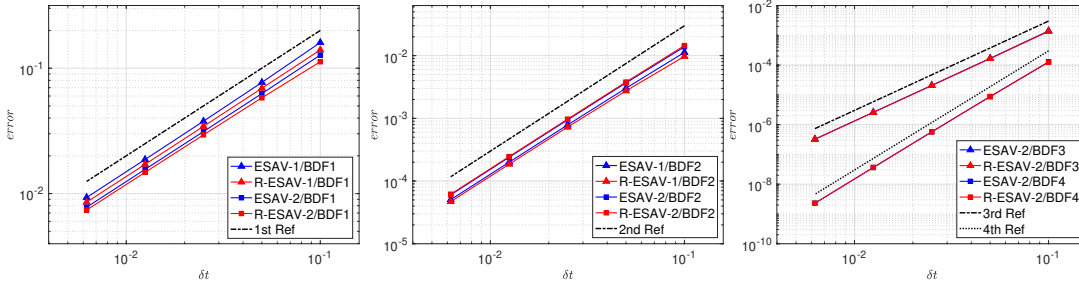


FIG. 1. *Example 1 (i)*. Convergence test for Allen-Cahn equation obtained by ESAB-1/BDF k , R-ESAB-1/BDF k ($k = 1, 2$), ESAB-2/BDF k and R-ESAB-2/BDF k ($k = 1, 2, 3, 4$) schemes.

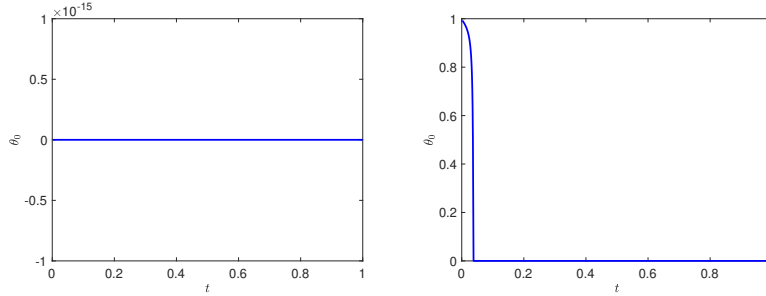


FIG. 2. *Example 1 (i)*. The evolution of relaxation factor θ_0^{n+1} with $\delta t = 1e - 3$. Left: R-ESAB-1/BDF2 scheme; right: R-ESAB-2/BDF2 scheme.

where (λ, ρ) are the polar coordinates of (x, y) . We set computational domain as $\Omega = [0, 1]^2$, the other parameters are $\sigma_0 = 0.01^2$, and Fourier modes are $N^2 = 128^2$. The computational solution of the semi-implicit/BDF2 scheme obtained by time step $\delta t = 1e - 5$ is regarded as the reference solution. It represents the L^2 -norm error of four numerical schemes we constructed above at $T = 200$ with various time steps in Table 1. It can be observed that, compared with ESAB-1 (resp. ESAB-2) schemes, R-ESAB-1 (resp. R-ESAB-2) schemes can noticeably reduce the error of the solution. The error of solution is large when the time step of ESAB-2 scheme is not sufficiently small, while R-ESAB-2 scheme can improve accuracy obviously. It also shows a comparison of energy (first), errors of energy (second) and the evolution of errors of energy at different time steps (third) for the constructed schemes in Fig. 3. Moreover the evolution of error of ξ^{n+1} is presented in Fig. 4, which indicates that the R-ESAB-1 (resp. R-ESAB-2) scheme can improve the accuracy compared with ESAB-1 (resp. ESAB-2) scheme and the error of ξ^{n+1} for R-ESAB-2 scheme will reach the machine accuracy after the simulation reaching the steady state.

Example 2. The Cahn-Hilliard equation

$$(4.4) \quad \frac{\partial \phi}{\partial t} = -M \Delta \left(\sigma_0 \Delta \phi + \frac{1}{\epsilon^2} (1 - \phi^2) \phi \right).$$

(i) We also choose (4.2) as the exact solution, and set model parameter to be $\sigma_0 = 0.04$, $M = 0.005$, $\epsilon = 1$. Fig. 5 shows the convergence rates of different schemes. We can observe similar results as those of the Allen-Cahn equation.

TABLE 1

Example 1 (ii). A comparison of L^2 -error obtained by four approaches based on BDF2 scheme for Allen-Cahn equation at $T = 200$ with various time steps.

	ESAV-1	R-ESAV-1	ESAV-2	R-ESAV-2
1E-1	9.49E-04	2.76E-04	0.98	1.01E-04
5E-2	8.43E-04	7.22E-05	1.07E-03	2.74E-05
1E-2	1.18E-04	2.94E-06	4.55E-05	1.01E-06
5E-3	3.53E-05	7.36E-07	2.29E-05	2.49E-07
1E-3	1.63E-06	2.96E-08	1.47E-06	9.88E-09

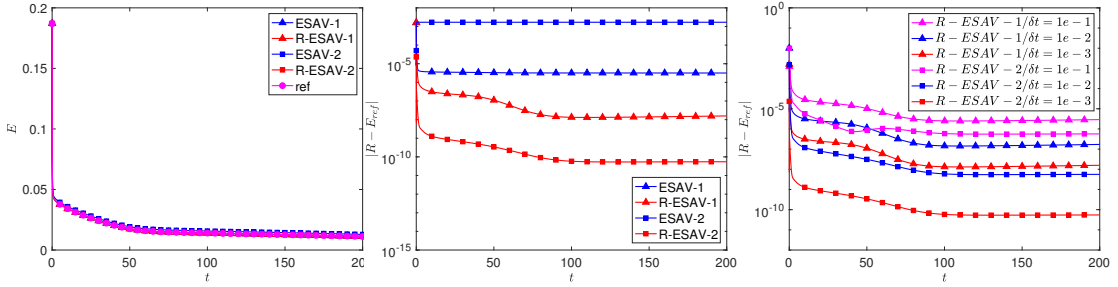


FIG. 3. Example 1 (ii). Allen-Cahn equation: a comparison of energy (first) and errors of energy (second) of four approaches based on BDF2 scheme; and a comparison of errors of energy of R-ESAV-1/BDF2 and R-ESAV-2/BDF2 schemes with various time steps (third).

(ii) We consider a rectangular array of 9×9 circles as the initial condition

$$(4.5) \quad \phi_0(\mathbf{x}, t) = 80 - \sum_{m=1}^9 \sum_{n=1}^9 \tanh \left(\frac{\sqrt{(x-x_m)^2 + (y-y_n)^2} - r_0}{\sqrt{2}\epsilon} \right),$$

where $r_0 = 0.085$, $x_m = 0.2 \times m$, $y_n = 0.2 \times n$ for $m, n = 1, 2, \dots, 9$. We set computational domain as $[0, 2]^2$, the other parameters are $M = 1e - 6$, $\sigma_0 = 1$, $\epsilon = 0.01$ and Fourier modes are $N^2 = 512^2$ in the simulations. The evolutions of an array of circles governed by Cahn-Hilliard equation using the R-ESAV-2/BDF2 scheme with $\delta t = 1e - 3$ are shown in Fig. 6.

Example 3. In this example, we consider the phase-field crystal model

$$(4.6) \quad \begin{cases} \frac{\partial \phi}{\partial t} = M \Delta \mu, & \mathbf{x} \in \Omega, t > 0, \\ \mu = (\Delta + \zeta)^2 \phi + \phi^3 - \epsilon \phi, & \mathbf{x} \in \Omega, t > 0, \\ \phi(\mathbf{x}, 0) = \phi_0(\mathbf{x}), \end{cases}$$

which is a H^{-1} -gradient flow associated with the total free energy as follows

$$(4.7) \quad E(\phi) = \int_{\Omega} \left(\frac{1}{2} \phi (\Delta + \zeta)^2 \phi + \frac{1}{4} \phi^4 - \frac{\epsilon}{2} \phi^2 \right) d\mathbf{x},$$

where $M > 0$ is the mobility coefficient. We set $M = 1$, $\zeta = 1$ in the following simulations.

(i) We first simulate the crystal growth in a super-cooled liquid in $2D$. We adopt the following initial condition

$$(4.8) \quad \phi(x_j, y_j, 0) = \bar{\phi} + \alpha_1 \left(\cos \left(\frac{\alpha_2}{\sqrt{3}} y_j \right) \cos(\alpha_2 x_j) - 0.5 \cos \left(\frac{2\alpha_2}{\sqrt{3}} y_j \right) \right), \quad j = 1, 2, \dots, 5,$$

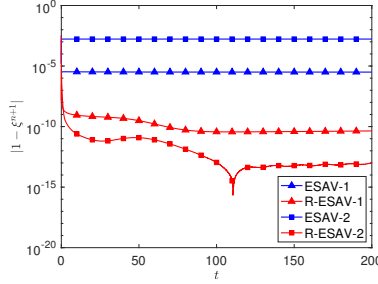


FIG. 4. Example 1 (ii). A comparison of the evolution of errors of ξ^{n+1} obtained by four approaches based on BDF2 scheme for Allen-Cahn equation.

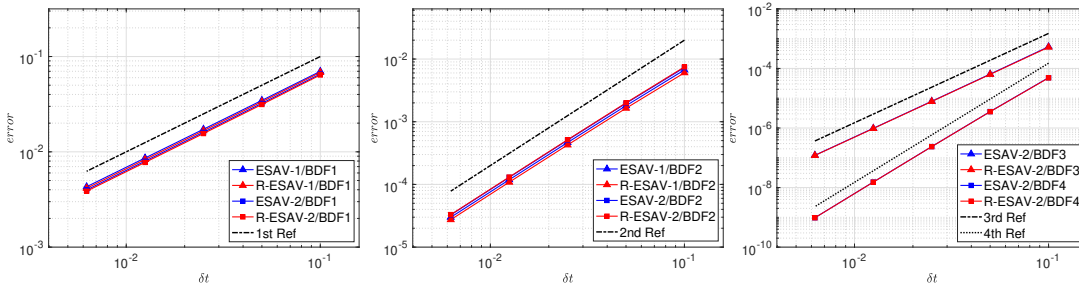


FIG. 5. Example 2 (i). Convergence test for Cahn-Hilliard equation obtained by ESAV-1/BDFk, R-ESAV-1/BDFk ($k = 1, 2$), ESAV-2/BDFk and R-ESAV-2/BDFk ($k = 1, 2, 3, 4$) schemes.

where x_j and y_j define a local system of Cartesian coordinates, which is oriented with the crystallite lattice. We choose the constant parameters as $\bar{\phi} = 0.285$, $\alpha_1 = 0.446$, $\alpha_2 = 0.66$. Then, we define five crystallites in five small square patches, each with a length of 40, located at (200, 200), (150, 600), (350, 400), (600, 300) and (550, 700) respectively. In order to produce crystallites with different orientations, we use the following affine transformation to generate rotation by five different angles $\rho = -\frac{3\pi}{4}, -\frac{\pi}{4}, 0, \frac{\pi}{4}, \frac{3\pi}{4}$ respectively

$$(4.9) \quad x_j(x, y) = x \sin(\rho) + y \cos(\rho), \quad y_j(x, y) = -x \cos(\rho) + y \sin(\rho).$$

We choose Fourier modes $N^2 = 1024^2$ to discretize the space and $\delta t = 0.02$ to discretize the time. And we set the other parameters as $\epsilon = 0.25$, $T = 800$. The relaxation parameter θ_0^{n+1} is also always zero in this example. We present the crystal growth in a super-cooled liquid by using the R-ESAV-1/BDF2 scheme for the PFC equation in Fig. 7, which indicate that the different alinement of the crystallites leads to defects and dislocations, just similar with those in [31, 18].

(ii) The initial condition is set to be

$$(4.10) \quad \phi(x, y, 0) = 0.07 + 0.07\delta,$$

where $\delta = rand(x, y)$ is the uniformly distributed random number in $[-1, 1]$ with zeros mean. Set the computational domain to $\Omega = [0, 128]^2$. The model parameter is chosen as $\epsilon = 0.025$, time step is $\delta t = 0.1$ and $N^2 = 256^2$ Fourier modes to discretize the space. It presents the configuration evolution in Fig. 8 and can observe from that uniform phase separation is formed finally. Similar computation results can be found in [20, 21].

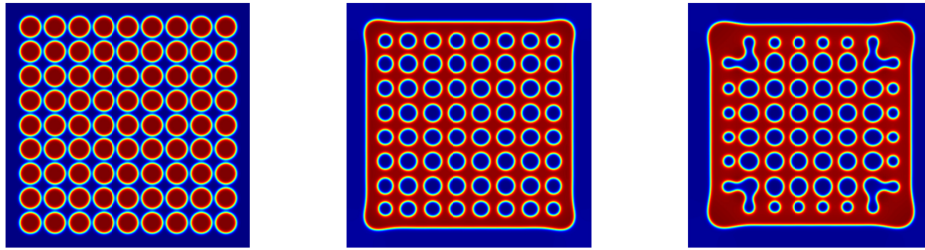
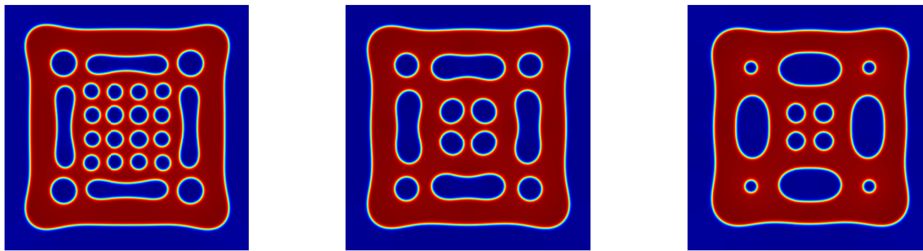
(a) profiles of $\phi = 0$ at $T = 0, 5, 10$ (b) profiles of $\phi = 0$ at $T = 20, 30, 50$

FIG. 6. *Example 2 (ii). The dynamic evolution of an array of circles governed by Cahn-Hilliard equation obtained by R-ESAV-2/BDF2 scheme.*

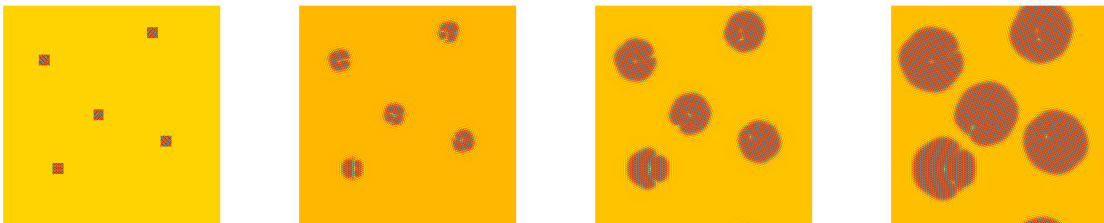
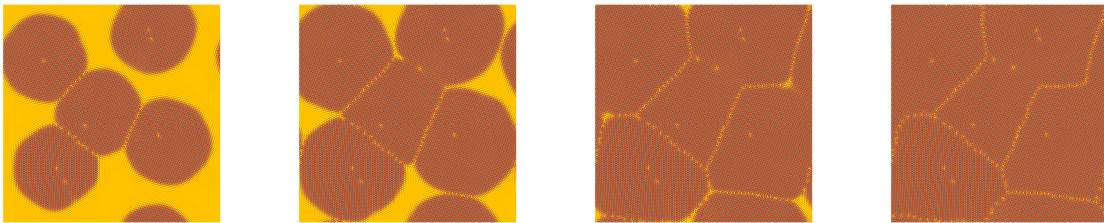
(a) profiles of ϕ at $T = 0, 100, 200, 300$ (b) profiles of ϕ at $T = 400, 500, 600, 800$

FIG. 7. *Example 3 (i). The 2D dynamic evolution of crystal growth in a supercooled liquid driven by the PFC equation obtained by R-ESAV-1/BDF2 scheme. Snapshots of the numerical solution ϕ at $T = 0, 100, 200, 300, 400, 500, 600, 800$, respectively.*

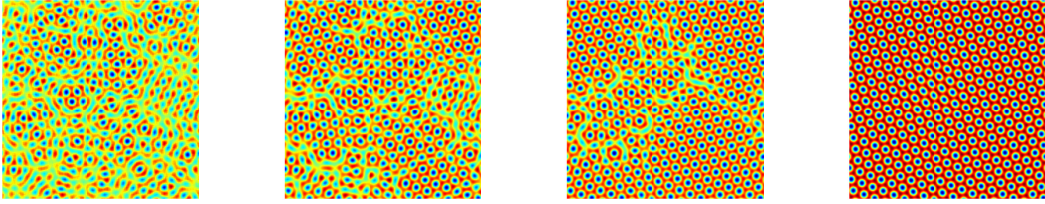
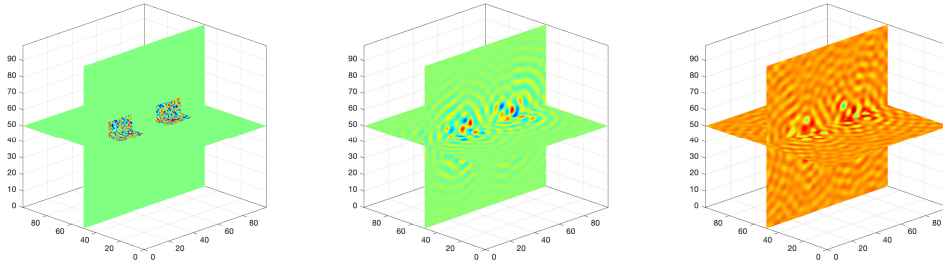


FIG. 8. *Example 3 (ii)*. The 2D configuration evolution driven by the PFC equation obtained by R-ESAV-1/BDF2 scheme. Snapshots of the numerical solution ϕ at $T = 400, 600, 1000, 2500$, respectively.

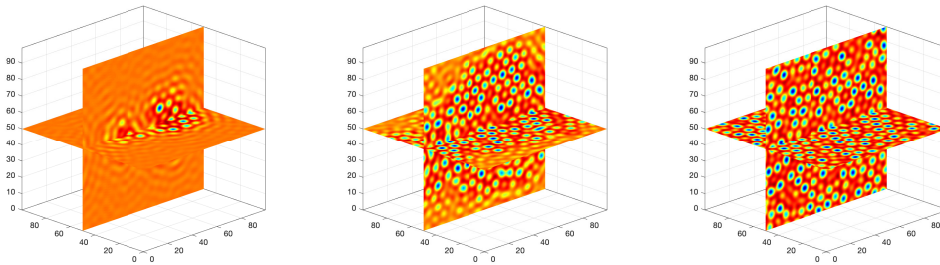
(iii) Then we simulate the crystal growth in a super-cooled liquid in 3D. We choose the computational domain $[0, 100]^3$ and the initial condition are two crystallites generated by

$$\phi(x, y, t = 0) = 0.285 + 0.01\delta.$$

The other parameters are chosen as $\epsilon = 0.25, \delta t = 0.02, T = 2000$. We adopt Fourier modes $N^3 = 128^3$ to discretize space. It can be observed that the effects of different arrangement of crystallites on the growth of the crystalline phase and the motion of crystal-liquid interfaces in Fig. 9, where these results are also consistent with those in [15].



(a) profiles of $\phi = 0$ at $T = 0, 60, 900$



(b) profiles of $\phi = 0$ at $T = 1000, 1100, 2000$

FIG. 9. *Example 3 (iii)*. The 3D dynamic evolution of crystal growth in a supercooled liquid driven by the PFC equation obtained by R-ESAV-1/BDF2 scheme. Snapshots of the numerical solution ϕ at $T = 0, 60, 900, 1000, 1100, 2000$, respectively.

(iv) Finally we study phase transition behaviors in 3D. The initial data are chosen as

$$\phi(x, y, t = 0) = \bar{\phi} + 0.01\delta,$$

and set computational domains $[0, 50]^3$. Other parameters are chosen as $\epsilon = 0.56, \delta t = 0.02, T = 3000$ and Fourier modes $N^3 = 64^3$. We present the steady state microstructure of the phase transition behavior for $\bar{\phi} = 0.20, 0.35$ and 0.43 , respectively in Fig. 10.

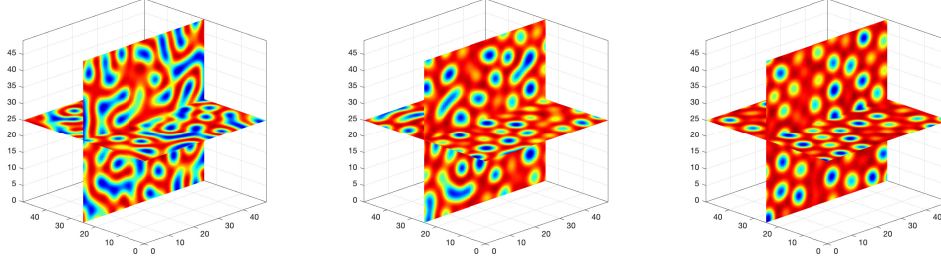


FIG. 10. *Example 3 (iv).* Evolution of ϕ in 3D driven by the PFC equation obtained by R-ESAV-1/BDF2 scheme with different $\bar{\phi}$ at $T = 3000$. First: $\bar{\phi} = 0.2$; Second: $\bar{\phi} = 0.35$; Third: $\bar{\phi} = 0.43$.

Example 4. In this example, we simulate the phase-field vesicle membrane (PFVM) model [4, 5] to demonstrate the effectiveness of the relaxed MESAV schemes. We consider the following penalized free energy to preserve the area and volume of vesicle membrane,

$$(4.11) \quad E(\phi) = E_b(\phi) + \frac{1}{2\sigma_1}(V(\phi) - v_0)^2 + \frac{1}{2\sigma_2}(S(\phi) - s_0)^2,$$

where σ_1, σ_2 are two small parameters, and v_0, s_0 are the initial volume and initial surface area, respectively. The definition of bending energy $E_b(\phi)$, volume $V(\phi)$ and surface area $S(\phi)$ of the vesicle are as follows

$$(4.12) \quad E_b(\phi) = \frac{\epsilon}{2} \int_{\Omega} \left(-\Delta\phi + \frac{1}{\epsilon^2}G(\phi) \right)^2 d\mathbf{x} = \frac{\epsilon}{2} \int_{\Omega} H^2 d\mathbf{x},$$

$$(4.13) \quad V(\phi) = \int_{\Omega} (\phi + 1) d\mathbf{x} \quad \text{and} \quad S(\phi) = \int_{\Omega} \left(\frac{\epsilon}{2} |\nabla\phi|^2 + \frac{1}{\epsilon} F(\phi) \right) d\mathbf{x},$$

where

$$H := -\Delta\phi + \frac{1}{\epsilon^2}G(\phi), \quad F(\phi) = \frac{1}{4}(\phi^2 - 1)^2, \quad G(\phi) := F'(\phi).$$

Then, the dynamic equation based on the above total energy can be described by

$$(4.14) \quad \begin{cases} \phi_t = -M\mu, \\ \mu = -\epsilon\Delta H + \frac{1}{\epsilon}G'(\phi)H + \frac{1}{\sigma_1}(V(\phi) - v_0) + \frac{1}{\sigma_2}(S(\phi) - s_0) (-\epsilon\Delta\phi + \frac{1}{\epsilon}F'(\phi)), \\ H = -\Delta\phi + \frac{1}{\epsilon^2}G(\phi), \end{cases}$$

with the periodic boundary condition, and M is the mobility constant. Then, it can easily obtain that the system (4.14) satisfy the energy law as follows

$$(4.15) \quad \frac{d}{dt}E(\phi) = -M\|\mu\|^2.$$

It can be observed that the system (4.14) contains two nonlinear terms associated with two small parameters ϵ and σ_2 respectively. Therefore, two SAVs are needed to introduce to deal with the different nonlinear terms. In the following simulations, we set computational domain as $\Omega = (-\pi, \pi)^3$, and the model parameters are $\sigma_1 = \sigma_2 = 0.01$, $\epsilon = \frac{6\pi}{128}$, $M = 1$. We compute the results using the R-MESAV-1/BDF2 scheme with time step $\delta t = 1e-4$ and $N^3 = 128^3$ Fourier modes.

(i) We first consider the interaction of four close-by spheres as the initial condition given by

$$(4.16) \quad \phi(x, y, z, 0) = \sum_{j=1}^4 \tanh \left(\frac{R_j - \sqrt{(x-x_j)^2 + (y-y_j)^2 + (z-z_j)^2}}{\sqrt{2}\epsilon} \right) + 3,$$

where $R_j = \frac{\pi}{6}$, $x_j = 0$, $(y_1, y_2, y_3, y_4) = (-\frac{\pi}{4}, \frac{\pi}{4}, -\frac{3\pi}{4}, \frac{3\pi}{4})$, and $z_j = 0$ for $j = 1, 2, 3, 4$.

Snapshots of iso-surfaces of $\phi = 0$ at $t = 0, 0.02, 1$ are presented in Fig. 11, which indicates that four small spheres gradually linked the shape of ‘ice sugar gourd’, and finally merge into a cylinder shape. The results are consistent with those presented in [5]. We also plot the evolution of relaxation factor θ_0^{n+1} in Fig. 12, and observe that, except the first several steps, θ_0^{n+1} always takes the value zeros.

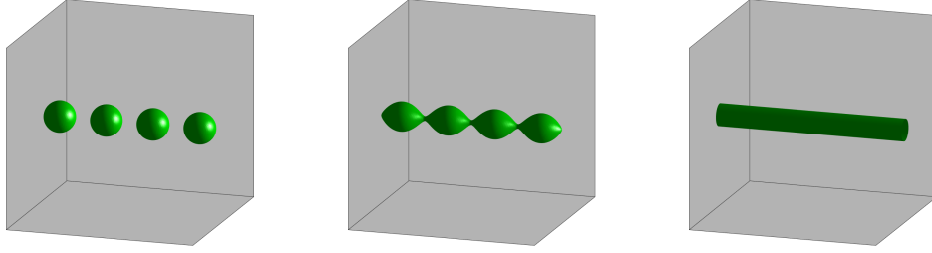


FIG. 11. Example 4 (i). The evolution of four close-by spherical vesicles. Snapshots of iso-surfaces of $\phi = 0$ driven by the PFVM equation at $t = 0, 0.02, 1$.

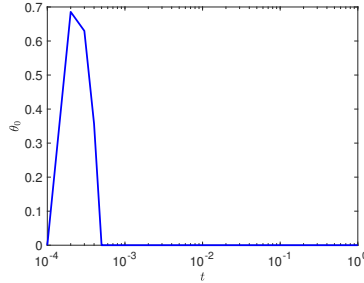


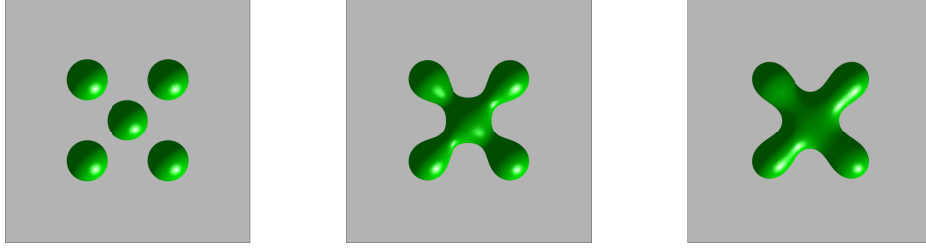
FIG. 12. Example 4 (i). The evolution of relaxation factor θ_0^{n+1} .

(ii) We simulate the evolution of five close-by spherical vesicles by choosing the initial condition

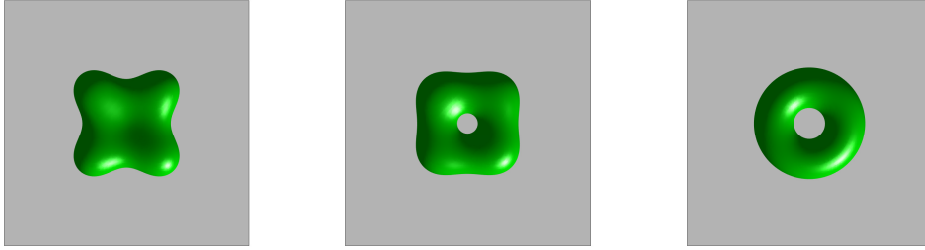
$$(4.17) \quad \phi(x, y, z, 0) = \sum_{j=1}^5 \tanh \left(\frac{R_j - \sqrt{(x-x_j)^2 + (y-y_j)^2 + (z-z_j)^2}}{\sqrt{2}\epsilon} \right) + 4,$$

where $R_j = \frac{\pi}{6}$, $z_j = 0$ for $j = 1, 2, \dots, 5$, $(x_1, x_2, x_3, x_4, x_5) = (-\frac{\pi}{3}, \frac{\pi}{3}, 0, -\frac{\pi}{3}, \frac{\pi}{3})$, and $(y_1, y_2, y_3, y_4, y_5) = (-\frac{\pi}{3}, -\frac{\pi}{3}, 0, \frac{\pi}{3}, \frac{\pi}{3})$.

We represent the evolution process in Fig. 13. It can be observed that five spheres connect within a small time interval, gradually form a doughnut shape which is a final state.



(a) profiles of $\phi = 0$ at $T = 0, 0.02, 0.05$



(b) profiles of $\phi = 0$ at $T = 0.2, 0.3, 1$

FIG. 13. *Example 4 (ii).* The evolution of five close-by spherical vesicles. Snapshots of iso-surfaces of $\phi = 0$ driven by the PFVM equation at $T = 0, 0.02, 0.05, 0.2, 0.3, 1$.

(iii) Then we consider a more complicated initial condition which is nine close-by spherical vesicles given by

$$(4.18) \quad \phi(x, y, z, 0) = \sum_{j=1}^9 \tanh \left(\frac{R_j - \sqrt{(x - x_j)^2 + (y - y_j)^2 + (z - z_j)^2}}{\sqrt{2}\epsilon} \right) + 8,$$

where $R_j = \frac{\pi}{6}$, $z_j = 0$ for $j = 1, 2, \dots, 9$, $(x_1, x_2, x_3, x_4, x_5, x_6, x_7, x_8, x_9) = (-\frac{\pi}{2}, 0, \frac{\pi}{2}, -\frac{\pi}{2}, 0, \frac{\pi}{2}, -\frac{\pi}{2}, 0, \frac{\pi}{2})$, and $(y_1, y_2, y_3, y_4, y_5, y_6, y_7, y_8, y_9) = (-\frac{\pi}{2}, -\frac{\pi}{2}, -\frac{\pi}{2}, 0, 0, 0, \frac{\pi}{2}, \frac{\pi}{2}, \frac{\pi}{2})$.

The evolutions of nine close-by spherical vesicles are demonstrated in Fig. 14, which represents that the initially nine spheres gradually connect with each other and finally form a big vesicle.

Example 5. In this numerical simulation, we test the Navier-Stokes equation.

(i) We start with the accuracy test. The right hand side is computed according to the following analytic solution

$$(4.19) \quad \begin{cases} p(x, y, t) = \exp(t) \sin(\pi y), \\ u_1(x, y, t) = \exp(t) \sin^2(\pi x) \sin(2\pi y), \\ u_2(x, y, t) = -\exp(t) \sin(2\pi x) \sin^2(\pi y), \end{cases}$$

the computational domain is $\Omega = (-1, 1)^2$, other parameters are chosen as $\nu = 0.1, T = 1$. We use Legendre spectral method to discretize space and $N^2 = 64^2$. The numerical results for BDF1 and BDF2 of Schemes I and II are presented in Tables 2-5 respectively. It can be seen that the errors of the solution will be greatly reduced by using the relaxation factor.

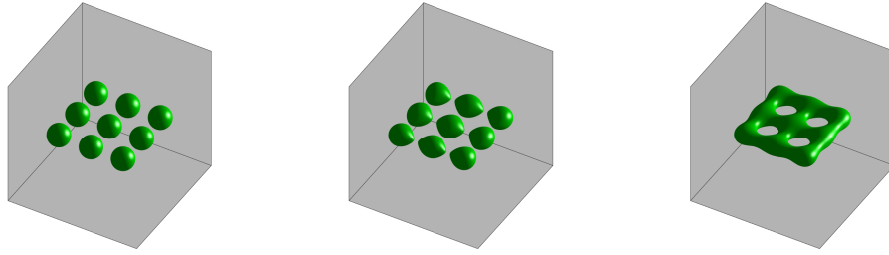
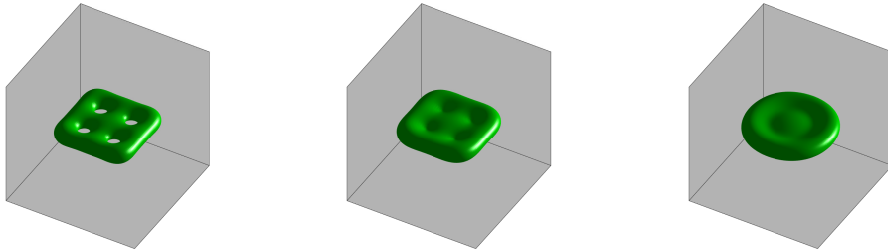
(a) profiles of $\phi = 0$ at $T = 0, 0.02, 0.05$ (b) profiles of $\phi = 0$ at $T = 0.1, 0.2, 1$

FIG. 14. *Example 4 (iii). The evolution of nine close-by spherical vesicles. Snapshots of iso-surfaces of $\phi = 0$ driven by the PFVM equation at $T = 0, 0.02, 0.05, 0.1, 0.2, 1$.*

(ii) Next we simulate double shear layer problem. We consider the Navier-Stokes equation with periodic boundary condition, and the initial condition provided by

$$(4.20) \quad \begin{aligned} u_1(x, y, 0) &= \begin{cases} \tanh(\sigma(y - 0.25)), & y \leq 0.5, \\ \tanh(\sigma(0.75 - y)), & y > 0.5, \end{cases} \\ u_2(x, y, 0) &= \epsilon \sin(2\pi x), \end{aligned}$$

where σ is the parameter of the shear layer width and ϵ is the size of the perturbation. We choose $\sigma = 30, \epsilon = 0.05$ and computational domain $\Omega = (0, 2)^2$ in the next simulations. We use Fourier modes $N^2 = 128^2$ and set $\delta t = 6.7e - 4$ to test the Navier-Stokes equation with $\nu = 5e - 5$. The vorticity contours of velocity field \mathbf{u} at $T = 1.2$ using BDF k ($k = 1, 2, 3, 4$) schemes are presented in Fig. 15. It can be observed that the BDF3 and BDF4 schemes give correct solutions, while the BDF1 scheme leads to a totally wrong result and the result of the BDF2 scheme is also inaccurate. The numerical phenomenon demonstrates the superiorities of high-order schemes. The evolution of contours of vorticity with $\nu = 1e - 4$, and $\delta t = 6e - 4$ obtained by BDF2 scheme is shown in Fig. 16. We can observe from the results that the vortex increases gradually.

5. Conclusions. In this paper, we constructed two kind of R-ESAV/BDF k schemes which can improve the accuracy significantly by introducing a relaxation factor to improve the accuracy for the classical SAV method. The constructed schemes are linear and unconditionally energy stable. They can guarantee the positive property of SAV without any assumption compared with R-SAV and R-GSAV approach. Moreover the constructed R-ESAV-2 approach is easy to construct high-order BDF k schemes and can be applied to general dissipative system. Finally we proved that the constructed RESAV scheme with relaxation are more accuracy and closer to original energy by using ample numerical examples.

TABLE 2

Example 5 (i). Convergence test for Navier-Stokes equation using Scheme I/BDF1 with and without relaxation.

δt	ESAV-2				R-ESAV-2			
	$\ e_{\mathbf{u}}\ _{L^2}$	Rate	$\ e_p\ _{L^2}$	Rate	$\ e_{\mathbf{u}}\ _{L^2}$	Rate	$\ e_p\ _{L^2}$	Rate
2.50E-2	4.29E-02	–	1.40	–	1.08E-02	–	2.62E-01	–
1.25E-2	1.96E-02	1.13	6.46E-01	1.11	4.85E-03	1.15	1.15E-01	1.19
6.25E-3	9.40E-03	1.06	3.10E-01	1.06	2.32E-03	1.06	5.35E-02	1.10
3.13E-3	4.61E-03	1.03	1.52E-01	1.03	1.14E-03	1.03	2.58E-02	1.05
1.56E-3	2.28E-03	1.01	7.52E-02	1.01	5.63E-04	1.01	1.26E-02	1.03

TABLE 3

Example 5 (i). Convergence test for Navier-Stokes equation using Scheme I/BDF2 with and without relaxation.

δt	ESAV-2				R-ESAV-2			
	$\ e_{\mathbf{u}}\ _{L^2}$	Rate	$\ e_p\ _{L^2}$	Rate	$\ e_{\mathbf{u}}\ _{L^2}$	Rate	$\ e_p\ _{L^2}$	Rate
2.50E-2	1.94E-03	–	4.47E-02	–	1.54E-03	–	9.25E-03	–
1.25E-2	4.64E-04	2.06	9.96E-03	2.17	3.88E-04	1.99	2.77E-03	1.74
6.25E-3	1.14E-04	2.02	2.40E-03	2.05	9.73E-05	1.99	8.79E-04	1.66
3.13E-3	2.84E-05	2.00	6.19E-04	1.96	2.46E-05	1.99	3.03E-04	1.54
1.56E-3	7.28E-06	1.97	1.70E-04	1.86	6.37E-06	1.95	1.07E-04	1.50

TABLE 4

Example 5 (i). Convergence test for Navier-Stokes equation using Scheme II/BDF1 with and without relaxation.

δt	ESAV-2				R-ESAV-2			
	$\ e_{\mathbf{u}}\ _{L^2}$	Rate	$\ e_p\ _{L^2}$	Rate	$\ e_{\mathbf{u}}\ _{L^2}$	Rate	$\ e_p\ _{L^2}$	Rate
2.50E-2	4.86E-01	–	9.34E-01	–	1.99E-01	–	2.89E-01	–
1.25E-2	3.12E-01	0.64	6.03E-01	0.63	9.51E-02	1.07	1.34E-01	1.11
6.25E-3	1.86E-01	0.75	3.58E-01	0.75	4.60E-02	1.05	6.37E-02	1.07
3.13E-3	1.03E-01	0.85	1.99E-01	0.85	2.26E-02	1.03	3.09E-02	1.04
1.56E-3	5.47E-02	0.91	1.05E-01	0.92	1.15E-02	1.02	1.52E-02	1.02

TABLE 5

Example 5 (i). Convergence test for Navier-Stokes equation using Scheme II/BDF2 with and without relaxation.

δt	ESAV-2				R-ESAV-2			
	$\ e_{\mathbf{u}}\ _{L^2}$	Rate	$\ e_p\ _{L^2}$	Rate	$\ e_{\mathbf{u}}\ _{L^2}$	Rate	$\ e_p\ _{L^2}$	Rate
2.50E-2	3.83E-02	–	6.23E-02	–	8.25E-03	–	1.59E-02	–
1.25E-2	7.60E-03	2.33	1.30E-02	2.26	2.05E-03	2.01	3.96E-03	2.00
6.25E-3	1.73E-03	2.14	2.98E-03	2.12	5.15E-04	2.00	9.93E-04	1.99
3.13E-3	4.13E-04	2.06	7.17E-04	2.06	1.29E-04	2.00	2.49E-04	2.00
1.56E-3	1.01E-04	2.03	1.76E-04	2.03	2.23E-05	2.00	6.24E-05	2.00

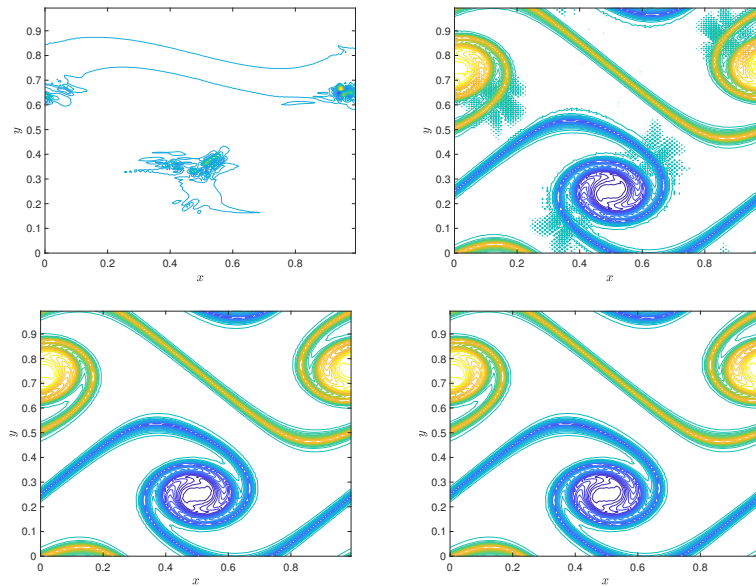
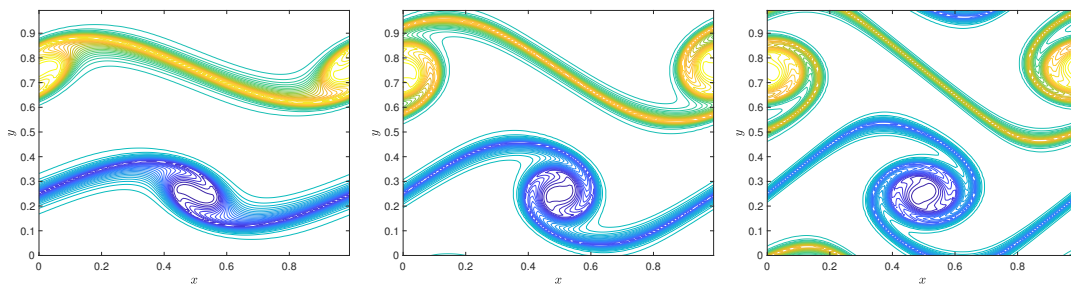
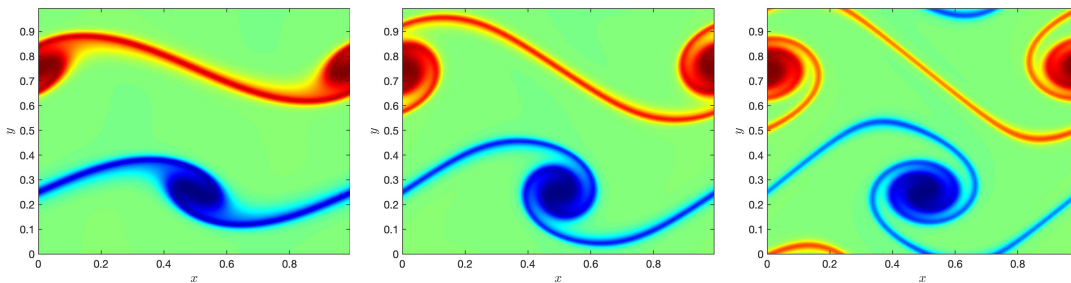


FIG. 15. Example 5 (ii). The vorticity contours at $T = 1.2$ with $\nu = 5e - 5$, and $\delta t = 6.7e - 4$ obtained by Scheme II/BDFk ($k = 1, 2, 3, 4$).



(a) contours of vorticity at $T = 0.8, 1, 1.2$



(b) color-filled contours of vorticity at $T = 0.8, 1, 1.2$

FIG. 16. Example 5 (ii). The evolution of vorticity with $\nu = 1e - 4$, and $\delta t = 6e - 4$ obtained by Scheme II/BDF2.

REFERENCES

- [1] Arvind Baskaran, John S Lowengrub, Cheng Wang, and Steven M Wise. Convergence analysis of a second order convex splitting scheme for the modified phase field crystal equation. *SIAM Journal on Numerical Analysis*, 51(5):2851–2873, 2013.
- [2] Qing Cheng, Chun Liu, and Jie Shen. A new Lagrange multiplier approach for gradient flows. *Computer Methods in Applied Mechanics and Engineering*, 367:113070, 2020.
- [3] Qing Cheng, Chun Liu, and Jie Shen. Generalized SAV approaches for gradient systems. *Journal of Computational and Applied Mathematics*, 394:113532, 2021.
- [4] Qing Cheng and Jie Shen. Multiple scalar auxiliary variable (MSAV) approach and its application to the phase-field vesicle membrane model. *SIAM Journal on Scientific Computing*, 40(6):A3982–A4006, 2018.
- [5] Qing Cheng and Jie Shen. Global constraints preserving scalar auxiliary variable schemes for gradient flows. *SIAM Journal on Scientific Computing*, 42(4):A2489–A2513, 2020.
- [6] Qing Cheng, Jie Shen, and Xiaofeng Yang. Highly efficient and accurate numerical schemes for the epitaxial thin film growth models by using the SAV approach. *Journal of Scientific Computing*, 78(3):1467–1487, 2019.
- [7] Qiang Du, Lili Ju, Xiao Li, and Zhonghua Qiao. Maximum principle preserving exponential time differencing schemes for the nonlocal Allen–Cahn equation. *SIAM Journal on Numerical Analysis*, 57(2):875–898, 2019.
- [8] Qiang Du, Lili Ju, Xiao Li, and Zhonghua Qiao. Maximum bound principles for a class of semilinear parabolic equations and exponential time-differencing schemes. *SIAM Review*, 63(2):317–359, 2021.
- [9] Charles M Elliott and AM Stuart. The global dynamics of discrete semilinear parabolic equations. *SIAM Journal on Numerical Analysis*, 30(6):1622–1663, 1993.
- [10] David J Eyre. Unconditionally gradient stable time marching the Cahn–Hilliard equation. *MRS Online Proceedings Library (OPL)*, 529, 1998.
- [11] Fukeng Huang and Jie Shen. Stability and error analysis of a class of high-order imex schemes for navier–stokes equations with periodic boundary conditions. *SIAM Journal on Numerical Analysis*, 59(6):2926–2954, 2021.
- [12] Fukeng Huang and Jie Shen. A new class of implicit–explicit BDFk SAV schemes for general dissipative systems and their error analysis. *Computer Methods in Applied Mechanics and Engineering*, 392:114718, 2022.
- [13] Fukeng Huang, Jie Shen, and Zhiguo Yang. A highly efficient and accurate new scalar auxiliary variable approach for gradient flows. *SIAM Journal on Scientific Computing*, 42(4):A2514–A2536, 2020.
- [14] Maosheng Jiang, Zengyan Zhang, and Jia Zhao. Improving the accuracy and consistency of the scalar auxiliary variable (SAV) method with relaxation. *Journal of Computational Physics*, page 110954, 2022.
- [15] Qi Li, Liquan Mei, Xiaofeng Yang, and Yibao Li. Efficient numerical schemes with unconditional energy stabilities for the modified phase field crystal equation. *Advances in Computational Mathematics*, 45(3):1551–1580, 2019.
- [16] Xiaoli Li and Jie Shen. Error Analysis of the SAV-MAC Scheme for the Navier–Stokes Equations. *SIAM Journal on Numerical Analysis*, 58(5):2465–2491, 2020.
- [17] Xiaoli Li and Jie Shen. On a SAV-MAC scheme for the Cahn–Hilliard–Navier–Stokes phase-field model and its error analysis for the corresponding Cahn–Hilliard–Stokes case. *Mathematical Models and Methods in Applied Sciences*, 30(12):2263–2297, 2020.
- [18] Xiaoli Li and Jie Shen. Stability and error estimates of the SAV Fourier-spectral method for the phase field crystal equation. *Advances in Computational Mathematics*, 46:1–20, 2020.
- [19] Lianlei Lin, Zhiguo Yang, and Suchuan Dong. Numerical approximation of incompressible Navier–Stokes equations based on an auxiliary energy variable. *Journal of Computational Physics*, 388:1–22, 2019.
- [20] Zhengguang Liu and Xiaoli Li. The exponential scalar auxiliary variable (E-SAV) approach for phase field models and its explicit computing. *SIAM Journal on Scientific Computing*, 42(3):B630–B655, 2020.
- [21] Zhengguang Liu and Xiaoli Li. A highly efficient and accurate exponential semi-implicit scalar auxiliary variable (ESI-SAV) approach for dissipative system. *Journal of Computational Physics*, 447:110703, 2021.
- [22] Jie Shen, Cheng Wang, Xiaoming Wang, and Steven M Wise. Second-order convex splitting schemes for gradient flows with Ehrlich–Schwoebel type energy: application to thin film epitaxy. *SIAM Journal on*

- Numerical Analysis*, 50(1):105–125, 2012.
- [23] Jie Shen and Jie Xu. Convergence and error analysis for the scalar auxiliary variable (SAV) schemes to gradient flows. *SIAM Journal on Numerical Analysis*, 56(5):2895–2912, 2018.
 - [24] Jie Shen, Jie Xu, and Jiang Yang. The scalar auxiliary variable (SAV) approach for gradient flows. *Journal of Computational Physics*, 353:407–416, 2018.
 - [25] Jie Shen, Jie Xu, and Jiang Yang. A new class of efficient and robust energy stable schemes for gradient flows. *SIAM Review*, 61(3):474–506, 2019.
 - [26] Jie Shen and Xiaofeng Yang. Numerical approximations of Allen-Cahn and Cahn-Hilliard equations. *Discrete & Continuous Dynamical Systems*, 28(4):1669, 2010.
 - [27] Jie Shen and Xiaofeng Yang. The IEQ and SAV approaches and their extensions for a class of highly nonlinear gradient flow systems. *Contemp. Math.*, 754:217–245, 2020.
 - [28] Xiaoqiang Wang, Lili Ju, and Qiang Du. Efficient and stable exponential time differencing Runge–Kutta methods for phase field elastic bending energy models. *Journal of Computational Physics*, 316:21–38, 2016.
 - [29] Ke Wu, Fukeng Huang, and Jie Shen. A new class of higher-order decoupled schemes for the incompressible Navier-Stokes equations and applications to rotating dynamics. *Journal of Computational Physics*, 458:111097, 2022.
 - [30] Xiaofeng Yang. Linear, first and second-order, unconditionally energy stable numerical schemes for the phase field model of homopolymer blends. *Journal of Computational Physics*, 327:294–316, 2016.
 - [31] Xiaofeng Yang and Daozhi Han. Linearly first-and second-order, unconditionally energy stable schemes for the phase field crystal model. *Journal of Computational Physics*, 330:1116–1134, 2017.
 - [32] Xiaofeng Yang and Lili Ju. Efficient linear schemes with unconditional energy stability for the phase field elastic bending energy model. *Computer Methods in Applied Mechanics and Engineering*, 315:691–712, 2017.
 - [33] Xiaofeng Yang and Haijun Yu. Efficient second order unconditionally stable schemes for a phase field moving contact line model using an invariant energy quadratization approach. *SIAM Journal on Scientific Computing*, 40(3):B889–B914, 2018.
 - [34] Yanrong Zhang and Jie Shen. A generalized SAV approach with relaxation for dissipative systems. *Journal of Computational Physics*, page 111311, 2022.
 - [35] Jingzhi Zhu, Long-Qing Chen, Jie Shen, and Veena Tikare. Coarsening kinetics from a variable-mobility Cahn-Hilliard equation: Application of a semi-implicit Fourier spectral method. *Physical Review E*, 60(4):3564, 1999.